MINIMIZING POWER CONSUMPTION OF THE ORGANIC OPTOELECTRONIC PULSE METER

ファハド, エス, エー, エルサムナ

https://doi.org/10.15017/2534467

MINIMIZING POWER CONSUMPTION OF THE ORGANIC OPTOELECTRONIC PULSE METER

BY

FAHED S. A. ELSAMNAH

KYUSHU UNIVERSITY

2019

MINIMIZING POWER CONSUMPTION OF THE ORGANIC OPTOELECTRONIC PULSE METER

BY

FAHED S. A. ELSAMNAH

A Thesis Submitted to the Interdisciplinary Graduate School of Engineering Sciences (IGSES) at Kyushu University in Partial Fulfillment of the Requirements for the Degree of
DOCTOR OF PHILOSOPHY
in Engineering

DEPARTMENT OF APPLIED SCIENCE FOR ELECTRONICS AND MATERIALS,
INTERDISCIPLINARY GRADUATE SCHOOL OF ENGINEERING SCIENCES,
KYUSHU UNIVERSITY
FUKUOKA, JAPAN
2019

MINIMIZING POWER CONSUMPTION OF THE ORGANIC OPTOELECTRONIC PULSE METER

BY

FAHED S. A. ELSAMNAH

A Thesis Submitted to the Interdisciplinary Graduate School of Engineering Sciences (IGSES) at Kyushu University in Partial Fulfillment of the Requirements for the Degree of
DOCTOR OF PHILOSOPHY
in Engineering

Under the Supervision of

Prof. Dr. Reiji Hattori

……

Professor
Department of Applied Science for Electronics and Materials
Faculty of Engineering Sciences,
Kyushu University

INTERDISCIPLINARY GRADUATE SCHOOL OF ENGINEERING SCIENCES, KYUSHU UNIVERSITY
FUKUOKA, JAPAN
July - 2019

ACKNOWLEDGEMENT

First of all, I would like to express my thankfulness to God for granting me the ability to finish my Ph.D. thesis. My foremost appreciation goes to Prof. Reiji Hattori, my supervisor, for his academic guidance and many other supports throughout my Ph.D. program. This thesis could not have been completed without his guidance and insightful instructions throughout my research. My special thanks are also due to our team research members; Anubha Bilgaiyan, Chang-Hoon Shim, Hiroshi Ishidai Muhamad Affiq, and Ryutaro Sugawara for their generous input and support during my research. Also, a special thank goes to my friend Abdul Moudood from Griffith University for his suggestions and comments during my study. I would like to express my acknowledgment for Prof. Yuichi Harada and Prof. Dong Wang for the time and effort to review my thesis and give valuable comments and suggestions which helped to improve the quality of the thesis. I also would like to thank all the colleagues at Hattori Lab who helped me to accomplish my research successfully.

I am very indebted to the Department of Applied Science for Electronics and Materials (ASEM) and to the dean of Interdisciplinary Graduate School of Engineering Sciences (IGSES), Prof. Hideharu Nakashima, for facilitating of my research work. I would like to thank the International Student and Researcher Support Centre and the Student Affairs Division of Chikushi Campus for their help and support during my study. I also would like to take this opportunity to thank the Japanese Ministry of Education, Culture, Sports, Science, and Technology (MEXT) for granting me a scholarship to support my research.

I am heavily indebted to my wife Noor and my parents, Samy and Nawal, and my brothers and sisters, for their continuous support and concern. My Ph.D. degree would not have been possible without the support of my wife, my parents and other members of my family.

DEDICATION

To my wife Noor and my daughter Yafa and all my family members, my teachers and my friends with gratitude for their inspiration, guidance and support.

ABSTRACT

A pulse oximetry sensor has become essential to medical electronics and wearable health monitoring devices. It is a noninvasive, inexpensive, convenient, and safe device for monitoring a person's health and avoiding any potential illness. The pulse oximeter is used to determine physiological parameters such as heart rate (bpm) and peripheral oxygen saturation (SpO_2) of the patient at all times based on the photoplethysmogram (PPG) method. PPG signal is an essential bio-signal that can be used for detecting several heart diseases. It has become fundamental to wearable health monitoring devices. This research aims to minimize the power consumption of the organic optoelectronic pulse meter sensor, develop the driver circuit of the pulse meter, and monitor the PPG waveforms wirelessly. A reflectance type organic optoelectronic pulse meter was proposed to measure the PPG signals. A red (625 nm) organic light-emitting diode (OLED) and an organic photodiode (OPD) sensitive at the aforementioned wavelength were fabricated monolithically on a glass substrate. The external quantum efficiency (EQE) of the OLED and the OPD were 7% and 37%, respectively.

In this research, several design structures were compared for minimizing the power consumption and noise level of the biosensor pulse meter. The comparison was done on two pairs of different shaped structures. In the first pair, one device had a circle-shaped OLED, 0.03 cm^2, in the center of the device and was surrounded by the OPD area of 0.16 cm^2, while the other device had OPD in the center and surrounded by OLED at same size area. In the second pair, both devices had a circle-shaped OLED in the center of the device and were surrounded by OPD. One device had an OLED area of 0.06 cm^2, while the other device had the half area. The gap distance between the OLED and OPD was 1.65 mm for the first device and 2 mm for the second one. Both devices have an OPD area of 0.16 cm^2. The power consumption and the signal-to-noise ratio (SNR) were evaluated for all devices' PPG signals, which were successfully acquired from fingertips and other body parts. Accordingly, the proposed reflectance-based organic pulse meter operated successfully at an ultra-low power consumption of 8 µW at 18 dB SNR and low power consumption of 0.1 mW at 62 dB.

The proposed organic pulse meter was implemented for wireless monitoring of the PPG signal and successfully presented compatible characteristics. Clear PPG waveforms were obtained from the portable pulse meter via Bluetooth low energy (BLE) at 500 SPS and 8-bit resolution on the receiver PC host. The maximum throughput data rate between the chip and the PC host was 256 kbps at the minimum connection interval of 7.5 ms. The proposed pulse meter showed accurate results of about 1.5% error of the pulse rate (PR) compared to the commercially reference we obtained. The SNR of the PPG signals were evaluated and compared for different parts of the body and successfully acquired clear PPG signals at those positions, where the best signal was obtained from the fingertips at an SNR of about 62 dB. Eventually, the proposed organic biosensor reduced the power consumption and improved the capability of the pulse meter for long-term use.

TABLE OF CONTENTS

LIST OF TABLES

Table No. Page No.

LIST OF FIGURES

Figure No. Page No.

LISTS OF ABBREVIATIONS

2D	two-dimensional
AC	alternating current
ADC	analog-to-digital converter
BLE	Bluetooth low energy
BPF	bandpass filter
bpm	beats per minute
CRC	cyclic redundancy check
dB	decibel
DC	direct current
DFT	discrete Fourier transform
DWT	discrete wavelet transforms
ECG	electrocardiogram
EQE	external quantum efficiency
FFT	fast Fourier transform
FIR	finite impulse response
GAP	generic access profile
GATT	generic attribute
HPF	high pass filter
HR	heart rate
ICA	independent component analysis
IPA	isopropyl alcohol
ITO	indium-tin-oxide
L2CAP	logical link control and adaptation layer protocol
LED	light-emitting diode
LPF	low pass filter
MCU	microcontroller unit
OLED	organic light-emitting diode
OPD	organic photodiode
PD	photodiode
PDU	protocol data unit
PLED	polymer light-emitting diode
PPG	photoplethysmogram
PR	pulse rate
SCB	serial communication block
SNR	signal-to-noise ratio
SpO_2	peripheral oxygen saturation
SPS	sample per second
TF	transfer function
TIA	transimpedance amplifier
UART	universal asynchronous receiver-transmitter

CHAPTER ONE:

INTRODUCTION

1.1 OVERVIEW OF PULSE METERS

In general terms, the pulse meter is a device used to measure the rhythmic contraction and expansion of an artery at each beat of the heart based on the photoplethysmogram (PPG) principle. Nowadays, pulse meter can be used as a wearable health-monitoring device which can promote public health by facilitating a person's health assessment based on their personal vital signs. It is a noninvasive, inexpensive, convenient, and safe device for monitoring a person's health and avoiding any potential illness. Several methods have been developed to measure heart rate, most of which are based on electrocardiogram (ECG), PPG, and the piezoelectric effect [1,2]. However, the ECG and piezoelectric sensors cannot be used to estimate the peripheral oxygen saturation (SpO_2). Moreover, the ECG and piezoelectric sensors are very sensitive to any artificial muscle movements which might be unsuitable to be used as wearable devices. While the pulse meter uses one light source to estimate the heart rate (HR) based on the PPG principle, it can estimate the SpO_2 by using two different wavelengths of light sources as a pulse oximeter.

The PPG signal is one of the crucial biosignals used for monitoring and evaluating the HR and SpO_2 of the patient at all times, [3,4]. Meanwhile, there is a significantly increased concern in monitoring human performance during physical activity to improve the wearable medical devices for home care. Nowadays, pulse oximeters are being developed for continuously monitoring vital human signs, as comfortably and noninvasively. Furthermore, the PPG sensor can be easily embedded into wearable devices such as wristbands, finger clips, and ear clips, [5,6].

In recent years, organic pulse oximeters, that depend on the organic light-emitting diode (OELD) and organic photodiodes (OPD), received so much attention from many researchers due to the advantages of the organic optoelectronic devices including the relatively low cost, simple fabrication and ability to be fabricated on flexible substrates for comfortable wearable medical devices. Additionally, the OPD can be easily fabricated on a large size area compared to the restricted size of the general silicon-based photodiode (PD) which makes the OLED and OPD a preferable option for wearable pulse oximeters, [7–9].

The system structure of the PPG signal detector that we proposed in this work for a reflectance-based organic optoelectronic pulse meter device consists of three main parts; organic optoelectronic devices, driver circuit including microcontroller unit (MCU), and a display media; PC or mobile phone, as illustrated in Figure 1.1. The OLED and the OPD are fabricated on the same substrate and fixed with the readout circuit using an aluminum case for easy measuring and more protection from the ambient noise.

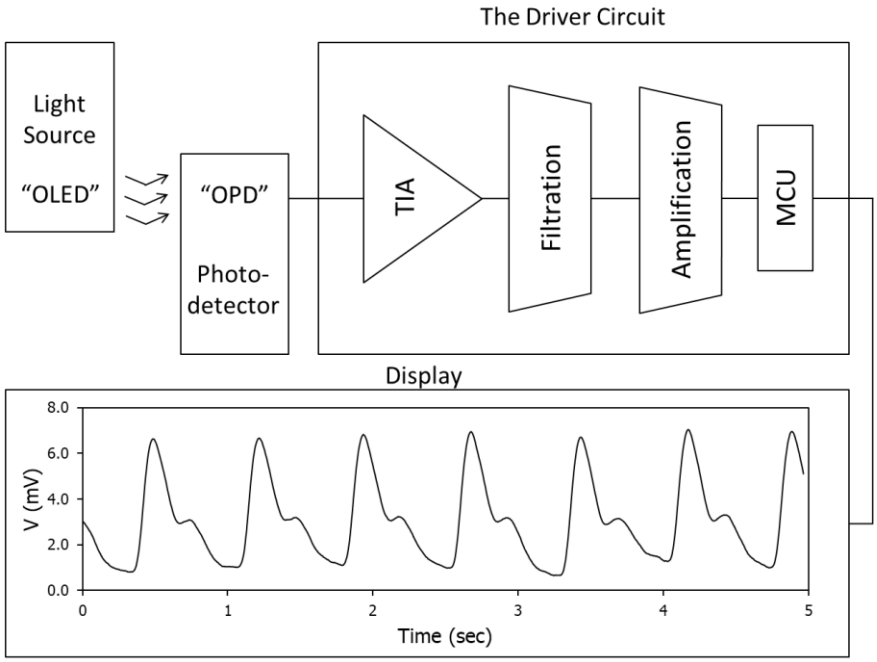

Figure 1.1: The system structure of the pulse meter device.

This thesis designs and fabricates an organic optoelectronic pulse meter device and evaluates its performance and signal quality. It also addresses the significance of the best designing of the OLEDs and the OPDs for pulse oximeter sensors in terms of power consumption and signal quality. The importance of using optical simulation is shown clearly in comparing the signal quality of an OLED with a high amount of light and an OLED with a low amount of light, and in comparing the signal quality of two devices with different gap distance between the OLED and the OPD. Therefore, designing an optimum OLED/OPD structure guided by optical simulation leads to the best results in terms of power consumption and signal quality.

1.2 MOTIVATION AND PROBLEM STATEMENT

The considerably increased concern for monitoring the vital signs in normal conditions as well as during physical activities has led to an enhancement of wearable medical devices and their performances for personal health care. Therefore, pulse oximeters, as wearable devices, have been developed to constantly monitor human performance both comfortably and noninvasively. Pulse oximeters provide accurate and reliable HR and SpO_2 measurements for medical diagnosis and evaluation where medical professionals must have trust and confidence in the results reported by their instruments in order to make an accurate assessment for their patients. Furthermore, the pulse oximeter can be a very useful tool in monitoring and detecting certain disorders such as sleep apnea, which is detected by measuring the SpO_2 in the blood.

Currently, there are various kinds of commercial pulse meter and pulse oximeter devices available on the market. However, there are still some issues with these kinds of pulse meters that need to be improved such as power consumption, signal quality, and the flexibility of the devices. Therefore, in order to make a flexible pulse meter, an

OLED and OPD are applied with the advantage of their flexibility and design freedom. Moreover, the relatively low cost, simple fabrication, and lower power consumption of the OLEDs and OPDs make them preferable options for wearable pulse meters.

1.3 RESEARCH OBJECTIVES

This research project aims to contribute to the development of a new organic optoelectronic design structure for minimizing the power consumption of the pulse oximeters. The objectives of this research project can be summarized as follows:

1. To design and fabricate organic optoelectronic devices that are used for developing the pulse meter.
2. To improve the power consumption of the proposed organic optoelectronic device.
3. To develop the driver circuit for the pulse meter with the minimum power consumption and monitor the PPG waveform wirelessly.
4. To evaluate the performance of the proposed portable device in terms of its precision and power consumption.

1.4 RESEARCH METHODOLOGY

This research has been focusing on reducing the power consumption and the noise level of the organic optoelectronic pulse meter device by improving the driving circuit and the design structure of the OLED and OPD with the guidance of optical simulation to get the best results. The methods used for this research are summarized as follows:

1. Performing a detailed investigation of previous and existing works related to developing pulse oximeter devices.

2. Conducting performance and characteristic evaluations of the fabricated OLED and OPD devices that guided by optical simulation. If the device does not meet the required characteristics, it will be refabricated.
3. Developing and evaluating the driver circuit for the organic optoelectronic device. If the driver circuit does not meet the specifications, the circuit will be redeveloped.
4. Comparing three different pulse meter design structures in order to improve power consumption and signal quality. One device has a circle-shaped OLED in the center of the device and surrounded by the OPD, while the second one has the opposite structure. The third device has a bigger circle-shaped OLED in the center of the device and surrounded by the OPD with a shorter gap distance between the OLED and the OPD.
5. Measuring the power consumption of the optoelectronic device, and measuring the signal-to-noise ratio (SNR) of the acquired PPG signal using the fast Fourier transform (FFT) technique.
6. Obtaining PPG signals from different parts of the body and evaluating the signal quality among them.
7. Developing a C# program for connecting the proposed potable pulse meter with the PC host via Bluetooth low energy (BLE) module in order to send the PPG waveforms wirelessly, and verifying the performance of the received wireless signal.
8. Publishing two journal papers, two conference papers, and writing the Ph.D. dissertation.

1.5 THESIS ORGANIZATION

This thesis consists of six chapters organized as follows:

Chapter One begins by giving a brief overview of the study, motivation and problem statement, objectives of the research and followed by the research methodology.

Chapter Two comprises literature review and related works, where the previous works on pulse oximeter systems, PPG principle, reflective type, transmissive type, organic optoelectronic, driving circuits, and digital filters are discussed in detail.

Chapter Three discusses the results of the optical simulation that lead to the best design structure in terms of power consumption and signal quality. Following that, the proposed design structure of the organic optoelectronic pulse meter and the characteristics of the device performance are presented.

Chapter Four discusses the system design which developed for the proposed organic pulse meter. The driver circuit and its stages were explained thoroughly. Also, Chapter Four illustrates the approach of measuring the SNR, the algorithm for measuring the heart rates, the data traffic of the BLE, and designing the digital filter that applied to the system.

Chapter Five contains the results of the proposed system's performance and accuracy. It compares the proposed design structures and discusses the results of the obtained PPG signal from several parts of the body along with comparing the PPG signal that has been acquired wirelessly via BLE.

Chapter Six presents the outcomes of the work presented in this dissertation. Thesis contribution to the current state of knowledge, recommendations, and future work are also presented.

CHAPTER TWO:

LITERATURE REVIEW

2.1 INTRODUCTION

This section presents the literature review and related works of pulse oximeter systems, where the previous works on developing the pulse meters, PPG principle, reflective and transmissive pulse meters, organic optoelectronic devices, wireless pulse meters, and the digital filters are discussed in detail.

2.2 PPG PRINCIPLE

The main function of the human heart is to pump oxygenated blood and nutrients to the body and eliminate carbon dioxide from the body. The order of cycling deoxygenated blood (Hb) over the lungs and pumping afresh oxygenated blood (HbO_2) to the body over the aorta is called the cardiac cycle. The HR is the frequency of cardiac cycles, defined as beats per minute (bpm). Any main change in the physical or mental state of a person normally changes the pulse. Thus, HR operates as one of the vital signs in evaluating the physical and mental status of a person. The HR can be measured accurately using electrical, optical, or strain sensors. In the case of electrical measurement, skin electrodes are used to get the depolarization signal from the heart muscles. This method is known as electrocardiography (ECG). On the other hand, in the case of optical measurement, the pulse meter is used to monitor the HR and cardiac cycle [10].

Pulse oximetry is a non-invasive method that allows monitoring the oxygen saturation of a patient's hemoglobin (Hgb). The Hgb is a protein which exists in the red blood cells, and it is responsible for transferring the oxygen to the whole body and

subtracting the carbon dioxide from the human body by transporting it to the lungs for exhalation process. It gives the red blood cells its color. Figure 2.1 shows the structure of Hgb, where each red blood cell contains thousands of Hgb molecules that carry oxygen to the body, [11].

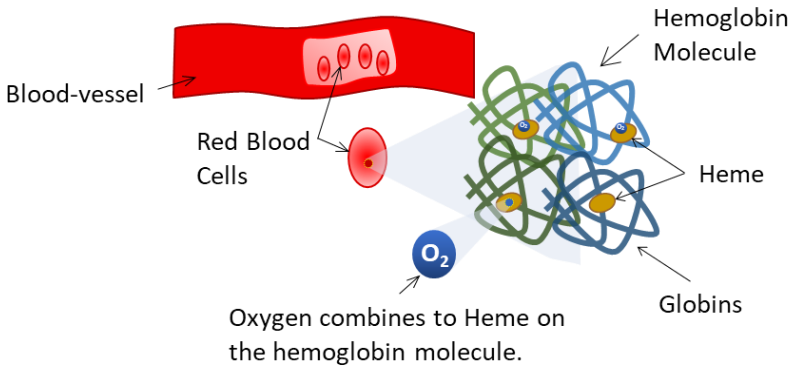

Figure 2.1: Structure of the hemoglobin molecule that exists in the red blood cells, [11]

The main role of red blood cells (erythrocytes) is to deliver oxygen to the body tissues and to bring waste carbon dioxide back to the lungs. Each Hgb molecule is comprised of four polypeptide chains called globins and four organic pigment molecules called hemes. Hence, one Hgb can hold four molecules of oxygen. There is one atom of iron in the center of each heme group, which can combine with one molecule of oxygen in the lungs and release oxygen in the tissues, [12].

There are two types of Hgb in the blood; oxygenated hemoglobin (HbO_2) and deoxygenated hemoglobin (Hb). Hgb merges with oxygen (O_2) to create HbO_2 in the lungs via a loading reaction. The HbO_2 is carried to the capillaries of the tissues where it separates to yield Hb and free O_2 molecules via an unloading reaction, and oxygen is used in mitochondria, [12]. Hb and HbO_2 have different optical absorbance coefficient in light wavelength spectrum, [3]. Therefore, pulse oximetry is mostly based on the absorbance characteristics at two different wavelengths where the oxygen saturation or

oxygenation (SpO_2) is the concentration of HbO_2 in the blood divided by the sum of the concentration of HbO_2 and Hb in the blood, which can be defined by Equation 2.1:

$$SpO_2 = \frac{[HbO_2]}{[HbO_2] + [Hb]} \times 100\ (\%) \qquad \text{Equation 2.1}$$

HbO_2 and Hb have different absorption spectra, as shown in Figure 2.2, where the plot of absorbance coefficient versus wavelength is based on Beer-Lambert law that related to the concentration of a solute to the intensity of light at a specific wavelength. In the red-light region, HbO_2 absorbs less light than Hb, while in the green-light region the reverse occurs.

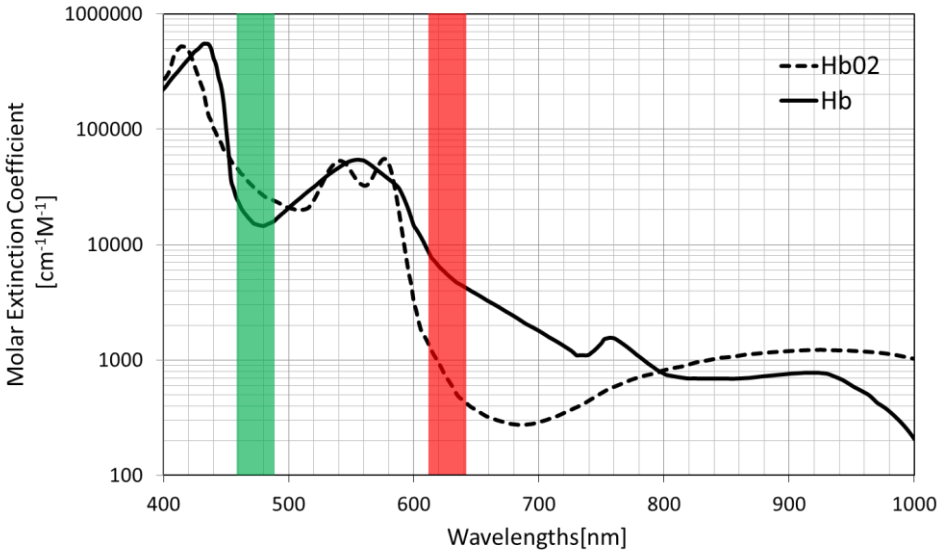

Figure 2.2: Light absorbance spectra of oxygenated hemoglobin (HbO_2) and deoxygenated hemoglobin (Hb), [13]

Beer-Lambert law stated that the intensity of light traveling through a medium decreases exponentially with distance [14], as described in Equation 2.2:

$$I_T = I_i \times e^{-\varepsilon(\lambda)CD} \qquad \text{Equation 2.2}$$

where; (I_T) is the intensity of transmitted light, (I_i) is the intensity of incident light, ($\varepsilon(\lambda)$) is the molar absorptivity, (C) is the concentration of the absorbent medium, and (D) is the optical path distance. Nonetheless, it is not easy to verify the exact intensity of the incident light applied. Furthermore, systole and diastole of heart pulse will cause small variations in the distance traveled by the light that is reflected. Therefore, Beer-Lambert's law needs to be adjusted for pulse oximetry and to apply empirically derived calibration curve. Thus, Equation 2.2 can be simplified to be independent of I_i and ΔD, as shown in Equation 2.3:

$$R = \frac{\alpha(\lambda_{Red})}{\alpha(\lambda_{Green})} = \frac{\ln(\Delta T_{Red})}{\ln(\Delta T_{Green})} = \frac{ln\left(\frac{I_2(\lambda_{Red})}{I_1(\lambda_{Red})}\right)}{ln\left(\frac{I_2(\lambda_{Green})}{I_1(\lambda_{Green})}\right)} \qquad \text{Equation 2.3}$$

where (R) is the ratio of the absorption ratio that is used to measure the SpO_2 on the calibration curve, as shown in Figure 2.3, (ΔT) is the change in transmission, ($\alpha(\lambda)$) is the molar absorptivity as a function of wavelength of red and green, $I_1(\lambda)$ is the peak value received from the photodetector of a single PPG pulse, and $I_2(\lambda)$ is the trough value of that pulse, [15].

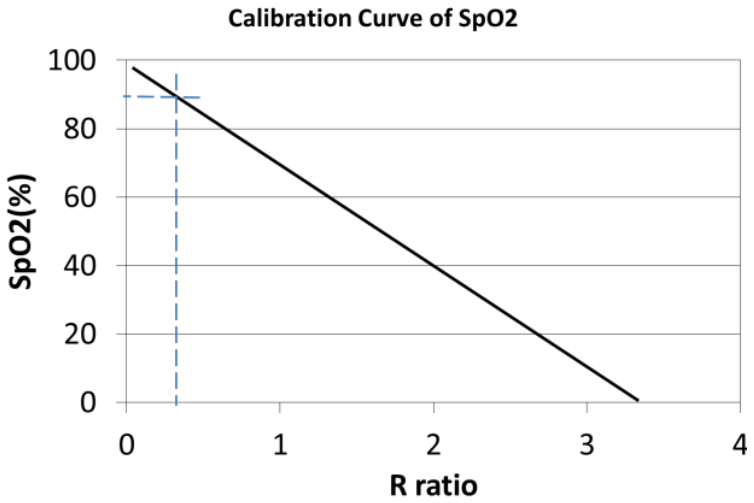

Figure 2.3: The calibration curve for estimating SpO_2 [16].

Depending on the sensing location and method, oxygenation can be categorized into three categories; venous oxygenation (SvO_2), tissue oxygenation (StO_2), and peripheral oxygenation (SpO_2). Among various oxygenation measurements, SpO_2 measurement is universal due to its noninvasive type. SpO_2 level should be about 95% in a healthy adult. If it decreases too low, below 80%, good organ function will be harmed, [3,17].

PPG principle consists of a light source and a light detector where the light transmits throughout the body tissues and reflects on the light detector, as shown in Figure 2.4. Apparently, when the heart beats, the blood volume of the arteries changes accordingly and causes variable light absorption, which leads to detect the change of reflected light as a PPG signal. In other words, the reflected or transmitted light from the pulse meter has a small pulsatile component in a pulse waveform, which is a result of the variations in the volume of arterial blood at the sensor site. This will cause changes in the light transmitted throughout the tissues, [4,18].

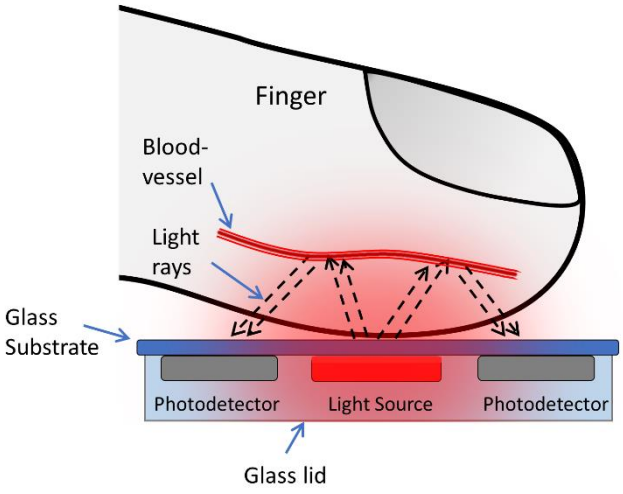

Figure 2.4: Acquiring photoplethysmogram (PPG) signal from reflectance mode.

The detected PPG signal comprises of an alternating (AC) component, which is due to variable absorption of the pulsatile arterial blood, and a steady-state (DC)

component from the venous, capillaries, tissue, bone and other non-pulsatile components, as shown in Figure 2.5, [14]. The AC component is the outcome of the light absorption by the arteries, while the DC component is the outcome of the light absorption by the body tissue and veins. Therefore, the pulsatile effect occurs only in the arteries but not in the veins or other non-pulsatile components, [19,20]. To put that into perspective, a pulse oximeter is based on two physical principles; spectrophotometric methodology and PPG principle to estimate the SpO_2, while the pulse meter relies on the PPG principle only.

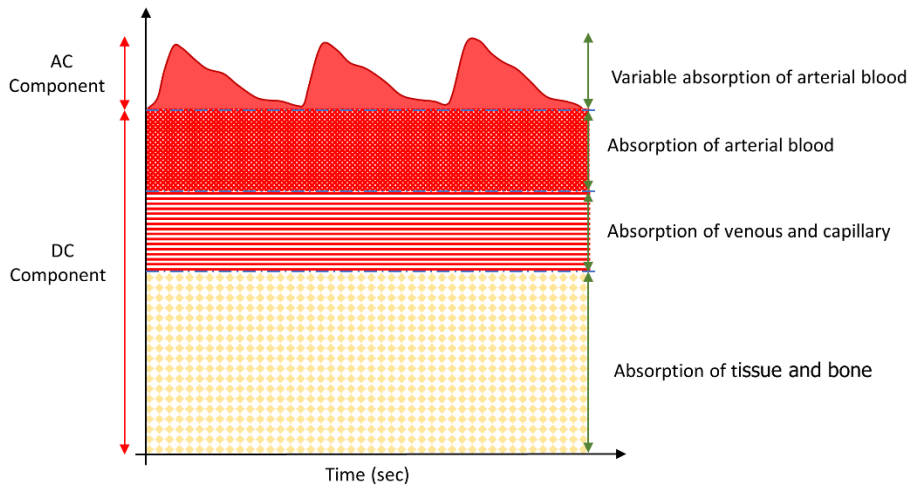

Figure 2.5: Schematic of light absorption in body tissues.

2.3 REFLECTIVE MODE VS TRANSMISSIVE MODE

To obtain a PPG signal from a pulse meter, there are two approaches that can be used: a reflective mode or a transmissive mode, as shown in Figure 2.6, which illustrates the differences between the two methods for an organic pulse meter.

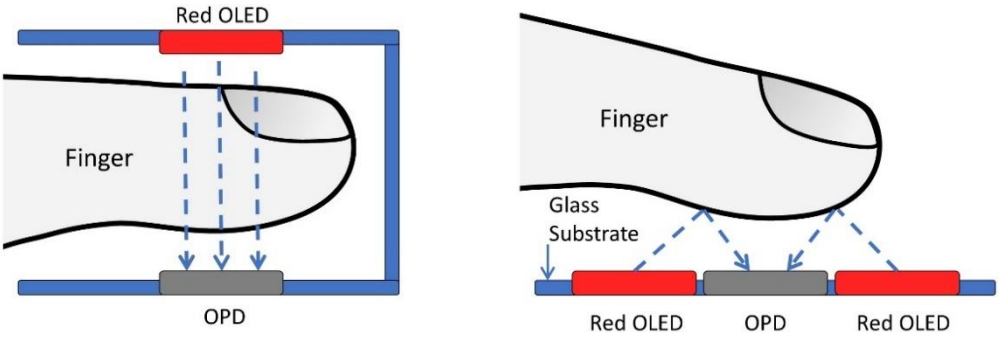

(**A**) (**B**)

Figure 2.6: Obtaining the PPG signal based on an organic pulse meter: (**A**) Transmissive mode; (**B**) Reflective mode.

The transmissive mode is based on the tissue transillumination where the light source and the detector are placed on opposite sides to each other, as shown in Figure 2.6A. The light from the OLED goes through the finger and is received on the OPD from the other side. On the other hand, the reflective mode, which is illustrated in Figure 2.6B, uses light reflection instead of tissue transillumination. The light source and the detector are both mounted side-by-side, where the OPD detector obtains the reflected light from the human skin. While the PD in the transmissive mode receives only the light that passes through many blood vessels in the finger, the PD in the reflective mode receives both the light that reflected from some blood vessels in the finger and the direct light from the LED. Consequently, the ratio of AC component to the DC component in the transmissive mode will be bigger than the ratio in the reflective mode, which means that the SpO_2 estimation will be more accurate in the transmissive mode. However, the transmissive mode is limited to be applied on terminal body parts such as fingertips, toes, and ear lobes. To overcome this limitation in the transmissive pulse oximeter, the reflective mode is used by taking advantage of the design freedom presented by the organic materials and fabricating it onto a flexible substrate. Therefore, the reflective pulse oximeter can be easily worn or attached to the human body. Several researchers

have started to work on the reflectance detection method [21,22], as the transmissive mode has been reported to be uncomfortable with limited usage. Furthermore, it gives inaccurate results if it was used in a cold environment or by a shaking finger. The reflective mode, on the other hand, has several advantages over the transmissive method, as it can be applied to different parts of the body, not only on the fingertips or the thin portion of the ear, to measure the PPG signal. However, in the reflective pulse oximeter, it is difficult to perform accurate oxygen saturation level measurement on several body locations, such as the torso or limbs, using the reflection mode due to the higher density of fat and lower density of blood vessels in those locations, [23]. Therefore, it is recommended to use the reflective pulse oximeter on body locations that have less density of fat such as the fingertips, wrist, arms, neck, and forehead.

2.4 RELATED WORKS ON PULSE OXIMETERS

Wearable medical devices require miniaturized, portable, and accurate healthcare monitoring devices to be compatible with the conventional one, which will lead to reducing healthcare expenditures and increasing the simplicity of health monitoring. Although the minimal functionality desired from pulse oximeter devices is the monitoring of vital signs, seemingly, they still require more reliability, rigidity, and accuracy in its sensitivity, circuit-board, power consumption and signal quality due to imperfect and varied skin structures from one person to another, noise and motion artifacts and the need for using the device for a long time, [24]. In that regard, several studies have been conducted in order to overcome these problems by proposing propitious solutions.

2.4.1 Organic Optoelectronics

One of the best advantages of the organic optoelectronic devices is the freedom of design, where the design engineer can make the best match between the OLED and OPD for improving the power consumption and the PPG signal quality. There are several proposed design structures in the literature. In [25], separated two square-shaped OLED devices and one rectangular-shaped OPD device were proposed as a transmissive mode pulse oximeter, while the authors of [26] proposed a monolithic device of array square-shaped OLEDs and OPDs for measuring the oxygen saturation and creating two-dimensional (2D) oxygenation maps. The configuration of an annularly-shaped photodiode (PD) ring and light-emitting diode (LED) located in the center was first proposed by the authors in [23] for improving the battery longevity of the inorganic reflective pulse oximeter. In [27], a circular-shaped OPD in the center of half-ring-shaped of red polymer light-emitting diode (PLED) and the second half-ring for green PLED design was proposed for the flexible reflective pulse oximeter. Also, a ring-shaped OPD surrounding a circular-shaped OLED was proposed by the authors in [28] for a flexible pulse oximetry sensor. They employed an optical simulation for deciding the best dimension area and the shortest gap between the OLED and the OPD where the relationship between the received radiant power with the gap distance was discussed without taking into consideration the DC noise. However, the PPG signal quality has not been adequately addressed in the previously proposed designs. Moreover, the dimension design, the material structure, and the characteristics of the OLED and OPD in this work are different than those in previous works. Consequently, this thesis proposed and compared different dimensions and material structures based on our works in [29–32] to improve the power consumption and the signal quality of portable

pulse meters, and highlighted the significance of the optical simulation in designing the OLED and the OPD devices.

There are several studies that have been carried out in the literature to improve the power consumption of the pulse meter. In [33], the study proposed a reflective pulse meter prototype with a total power of 40 mW, with the LED driving current between 17.4 ~ 50 mA. In contrast, the authors of [34] proposed an analog single-chip pulse oximeter that was implemented with 4.8 mW of total power consumption required of the LED power and the processing power chips. A fully integrated pulse oximeter front-end with about 1 mW of total power consumption, 0.31 mW for the LEDs, and 0.53 mW for the front-end was proposed in [35]. For improving the flexible pulse oximeter, a promising result of the average OLED's power consumption of 0.097 mW, at a full-duty cycle, was reported in [28]. While this thesis presenting the power consumption of the previous works on the pulse oximeter, which requires two light sources, it is worth mentioning that the proposed pulse meter in this work requires a single light source that leads to half the power consumption of two light sources when they operate at the same time with a full-duty cycle.

The organic pulse meter would be able to reduce the power consumption, while the inorganic pulse meter would not because it uses an inorganic PD which has a small rigid detection area and if the PD region area increased, the pulse meter would be uncomfortable for use. For that reason, the light intensity of the LED should be increased instead of increasing the area of the PD, which means more current consumption is needed. Furthermore, the PD requires a bias to work, which means more power will be consumed. Whereas in the organic materials, the surface area of the OPD can be increased at a zero-bias condition and collect many reflected photons from the

skin on the OPD. Moreover, the organic material can be deposited on a flexible substrate for a comfortable wearable pulse meter device.

2.4.2 Wireless Monitoring

Monitoring the PPG signal wirelessly requires considering the reduction of the wireless pulse meters device's power consumption, which is battery operated. That is to say, the size and weight of the device are predominantly determined by the size and weight of the battery. Therefore, decreasing power consumption is the top priority in developing wireless pulse meters.

In the literature, there are several studies that have attempted to develop a wireless monitoring pulse meter and solve several problems associated with it, such as signal quality and power consumption. In [36], the study proposed a compact portable module composed of photodetectors array, which was distributed radially around LEDs and sent the PPG signal via the Zigbee protocol wireless module. The chip consumed 38 mA for transmitting data and 37 mA for receiving data. The LEDs consumed about 38 mW in red LED, and 26 mW in IR LED. A wireless PR and SpO_2 monitoring system presented by the study in [37], where the proposed system connected to a local wireless network through Wi-Fi technology and the information was transmitted in real-time to a webpage for remote monitoring. The current consumption of that wireless MCU chip was 229 mA for TX traffic and 59 mA for RX traffic. Other researchers proposed wireless pulse oximeters but without mentioning the power consumption of the proposed device such as the study in [38] where authors proposed a wireless ring-type pulse oximeter with multi-detectors for sending the signal to the host system via Bluetooth, while the authors of [39] proposed a PPG wireless monitoring devices embedded in hat and glove and send the signal via Bluetooth. However, monitoring the

PPG signal wirelessly was not adequately addressed in the previous researches and prototypes for the signal quality. Moreover, the previously proposed devices for wireless monitoring still impractical for long term use. Therefore, the pulse meters, as wearable medical devices, are required to be miniaturized, portable and monitored wirelessly in order to provide more freedom and to be more comfortable and compatible with the conventional one, which will lead to increasing the simplicity of health monitoring.

2.4.3 Digital Filters

The PPG signal can be contaminated by noises from different kinds of sources such as motion artifacts, electronic noises, and high-frequency noises from the ambient light fixture and appliances. Consequently, extensive works have been done on denoising the PPG signals with several noise reduction techniques such as discrete wavelet transform (DWT) [40], independent component analysis (ICA) [41], and morphological characteristics comparison [42]. In [43], sporadic noise was reduced from a continuous periodic signal after applying a cluster analysis for picking similar replications or pulses from a periodic signal, while in [44], a pattern recognition filtering system for PPG and ECG signals was proposed. However, it is difficult to implement these methods into wearable devices due to their requirements and complexity. In this work, we implemented a finite impulse response (FIR) digital filter in order to improve the signal's quality because of its efficacy in the embedded systems.

2.5 SUMMARY

This chapter has discussed in detail the related works on the pulse oximeter systems, spectrophotometric methodology, PPG principle, reflective and transmissive

mode, organic optoelectronic, wireless pulse meters, and the digital filters. It summarized the previous works and contributions on developing the pulse meters.

CHAPTER THREE:

THE ORGANIC OPTOELECTRONIC DEVICES

3.1 INTRODUCTION

This section describes the optical simulation used for the design structure and defines the characteristics of the organic optoelectronic device, and lastly explains the driving circuit for the proposed device.

Three different design structures were fabricated and named as Device-A, Device-B, and Device-C. In Device-A, a circle-shaped red OLED was set in the center of the pulse meter with a total emitting area of 0.03 cm^2 and surrounded by a ring-shaped OPD with a surface area 0.16 cm^2, whereas in Device-B, a circle-shaped OPD was set in the center and surrounded by a ring-shaped red OLED with areas of 0.03 cm^2 and 0.16 cm^2, respectively. Device-C had a circle-shaped OLED, 0.06 cm^2, at the center and was surrounded by a ring-shaped OPD area of 0.16 cm^2. The gap distance between the OLED and OPD was 2 mm, 2 mm and 1.65 mm for Device-A, Device-B and Device-C, respectively. The rationale behind the use of the ring-shaped OPD structure that surrounds the OLED was to allow the OPD to collect the reflected photons from the skin efficiently.

3.2 OPTICAL SIMULATION

In order to get the best OLED and OPD design for improving the power consumption and quality of the PPG signal, a simplified finger model and OLED/OPD model were simulated optically by LightTools software (Synopsys, Inc., California, USA). The simulator traces the light rays using the ray-tracing method in combination with the Monte Carlo method, where three different design structures of the pulse meter

were simulated: Device-A, Device-B, and Device-C. The finger model was simplified into a four-layer structure of the skin, subcutaneous adipose tissue, muscle, and bone. The optical parameters of these layers were approximated from the literature in [45–48], and are shown in Table 3.1 where the refractive index of the material describes how fast light propagates through the material. The Henyey–Greenstein function was used to approximate the angular scattering dependence of single scattering events in biological tissues. The thickness of each layer was approximately assumed as 2 mm, 2.5 mm, 3 mm and 6 mm, respectively. The distribution of the light rays from the OLED into the human body and the reflection on the OPD were illustrated in Figure 3.1. In the model, the arterial blood vessels were assumed to be included in the skin and the subcutaneous adipose tissue for simplicity. The pulse meter model was composed of a light object source (625 nm) that represented the red OLED, and a surface receiver that represented the OPD. The dimensions of the OLEDs and OPDs design structures for all devices are illustrated in Figure 3.2, which demonstrates that Device-A was designed to be opposite of Device-B, and the area of the OLED in Device-C was designed to be double the size of that in Device-A in order to evaluate the effect of increasing the light source and decreasing the gap distance between the OLED and the OPD.

Table 3.1: Summary of the approximated optical parameters of a human finger.

Tissue	**Wavelength (nm)**	**Index of refraction (n)**	**Henyey-Greenstein (g)**	**Absorption Coefficient (Ua) in mm^{-1}**	**Scatter Coefficient (Us) in mm^{-1}**	**Thickness (mm)**
Human skin	625	1.55	0.81	0.27	18.7	2
Subcutaneous fat	625	1.44	0.9	1.14	12.8	2.5
Muscle	625	1.37	0.9	0.56	64.7	3
Bone	625	1.37	0.9	0.04	19.5	6

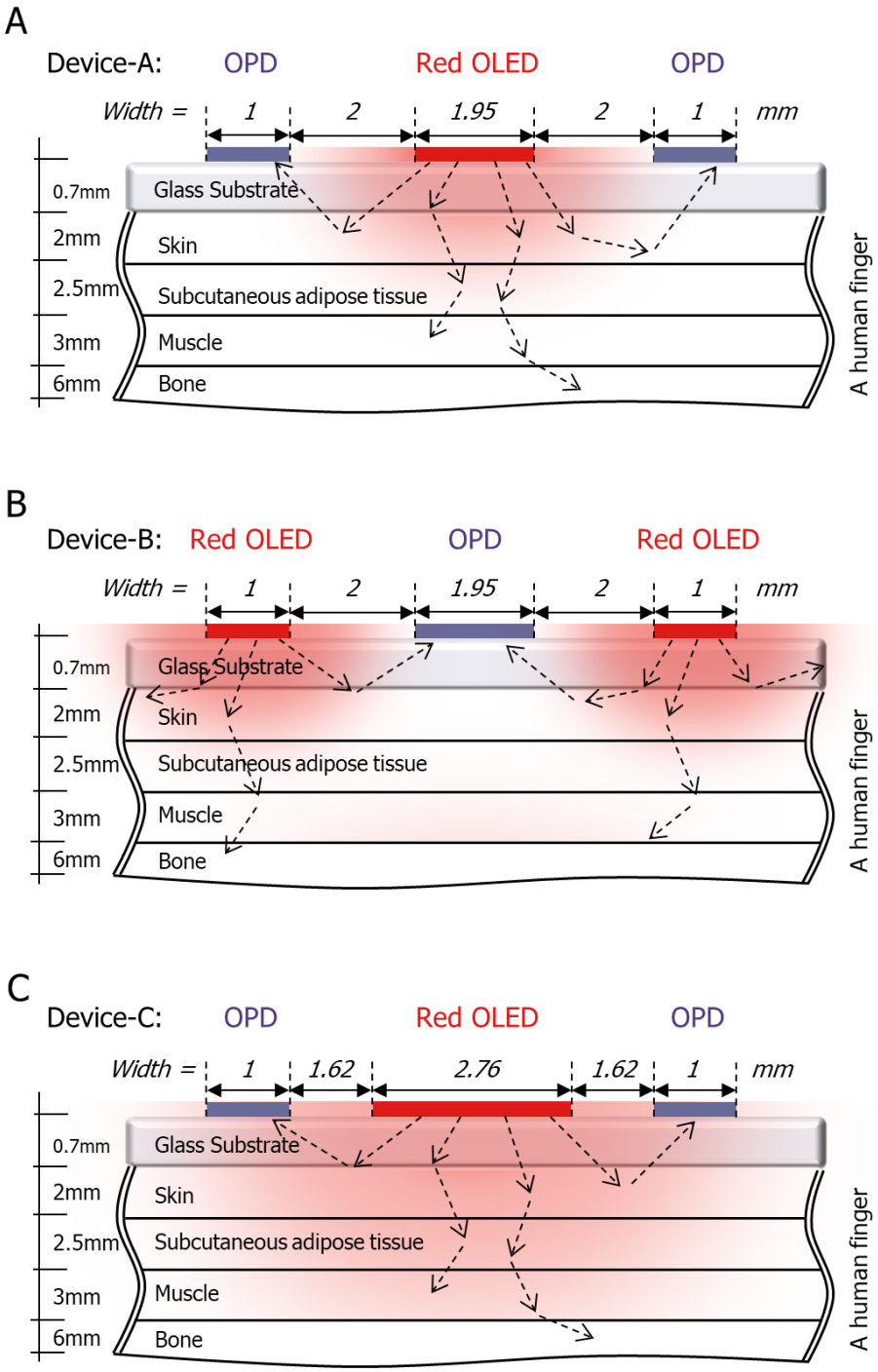

Figure 3.1: A simplified finger schematic model with the organic light-emitting diode (OLED) as the light object source and the organic photodiode (OPD) as the surface receiver for (**A**) Device-A; (**B**) Device-B and; (**C**) Device-C.

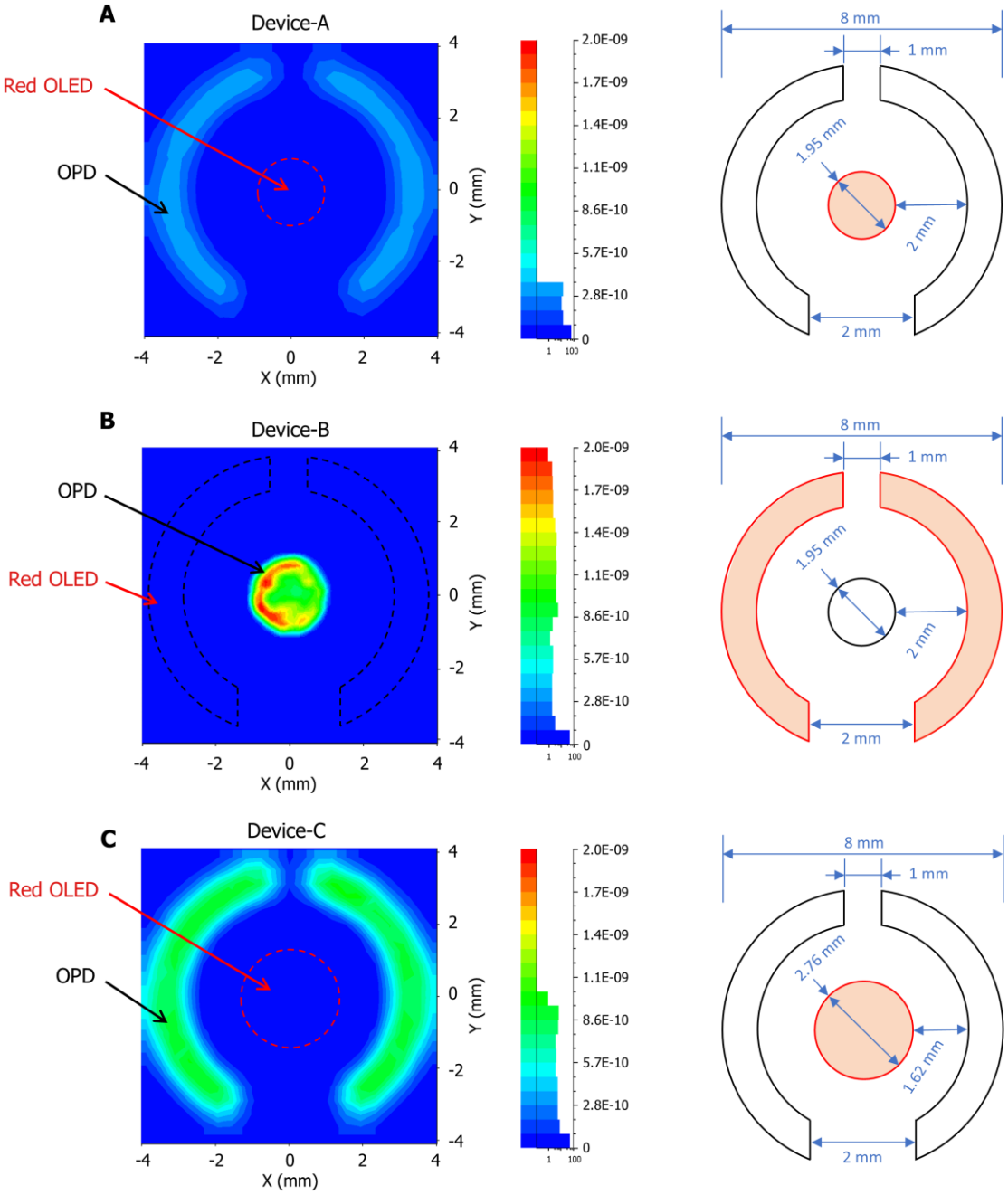

Figure 3.2: The optical simulation results at the receiver's surface in Watt per mm^2 and the dimensions of the OLED and OPD design structures for (**A**) Device-A; (**B**) Device-B and; (**C**) Device-C.

The light ray's energy is determined, in the optical simulation, by the source's power and the number of rays emitted. The radiant powers of the light object source of Device-A, Device-B and Device-C were assumed, based on our OLED device (625 nm) measurements, to be 1.4 µW, 7.5 µW, and 2.8 µW, respectively. The simulation traced

one million rays in each device. According to the simulation results in Figure 3.2, the maximum estimated irradiance on the OPD area of Device-A, Device-B and Device-C were 3.7×10^{-10} W/mm^2, 2×10^{-9} W/mm^2 and 9.8×10^{-10} W/mm^2, respectively. While the simulation presented an unequal irradiance distribution due to the spline effect of the ray simulation, we assumed the maximum irradiance was distributed equally. Therefore, the total power received of Device-A, Device-B and Device-C will be 5.9×10^{-9} W, 6×10^{-9} W and 15.6×10^{-9} W, respectively, which is expected to provide closer values of the PPG amplitude from the OPD devices. To put that into perspective, 0.42% of total light rays reflected on the OPD of Device-A, and just 0.1% of the total light rays reflected on the OPD of Device-B, while Device-C received the highest percentage of 0.55% from the total light rays on the OPD. In these simulation results, when the gap between the OLED and the OPD was decreased from 2 mm in Device-A to 1.62 mm in Device-C, the total power increased to more than double, which means that the amplitude of the PPG in Device-C was expected to be bigger than the amplitude in Device-A and Device-B. Therefore, from these three design structures, we conducted a comparison in order to choose the best one in terms of power consumption and signal quality.

3.3 CHARACTERIZATION OF THE ORGANIC OPTOELECTRONIC DEVICES

The good characteristics of the organic optoelectronic device improve the signal's quality of the pulse meter device, which in turn will provide accurate measurements in the medical examinations. As a monolithic device, the OLED and the OPD were deposited onto the same 0.7 mm thick glass substrate. For simplicity of the structure of the device and future fabrication, identical red OLED and OPD structures, shown in

Figure 3.3A, were fabricated on the same substrate. The organic material structure of the OLEDs and OPDs were the same for Device-A, Device-B, and Device-C, as shown in Figure 3.3B.

3.3.1 OLED Characterization

Organic LEDs have many advantages over LEDs, despite the fact that they have a shorter lifetime. OLEDs are relatively easy to produce, flexible, foldable, transparent, and capable of fast switching. The very thin organic and flat layer of the OLED device, compared to the LED, makes it applicable for fabrication onto a flexible substrate, which will be comfortable when placed on the human skin. OLED provides a suitable light intensity which will help in acquiring an accurate and strong signal due to the large reflective area of the OPD. Moreover, they are lower cost and consume less power. This has made organic light-emitting diodes (OLEDs) and OPDs preferable for use in wearable pulse oximeters [7–9].

In this work, three different pattern monolithic devices, Device-A, Device-B, and Device-C, were fabricated. The red OLED and the OPD were placed on the same 0.7 mm thick glass substrate, as shown in Figure 3.3A. The red OLED was adopted in this work due to its advantages over other OLEDs colors including the green OLED and near-infrared (NIR) OLED. In the case of green OLED, the green light has a shorter wavelength that is efficiently absorbed through the skin, which leads to producing a higher SNR level than the red OLED. However, absorbing more light through the skin, especially darker skin where the shorter wavelengths of light are strongly absorbed by melanin [49], limits the depth that light can pass through, hence, weakens the strength of the PPG signal [50]. Based on that, green OLEDs will face some challenges when they are used as a light source for wearable pulse oximeters. In the case of the NIR

OLED, the NIR region of the spectrum has a longer wavelength, which leads to increasing the penetration depth of the light in the human body. However, the external quantum efficiency (EQE) in this region is significantly lower than the OLED in the visible region. Moreover, fabricating NIR OLED/OPD device is difficult and still under research and development due to instability issues and unavailability of appropriate materials. The NIR OLED/OPD materials are less stable than the red OLED/OPD materials. Also, it is difficult to synthesize low bandgap material that is required for OLED and OPD [51,52].

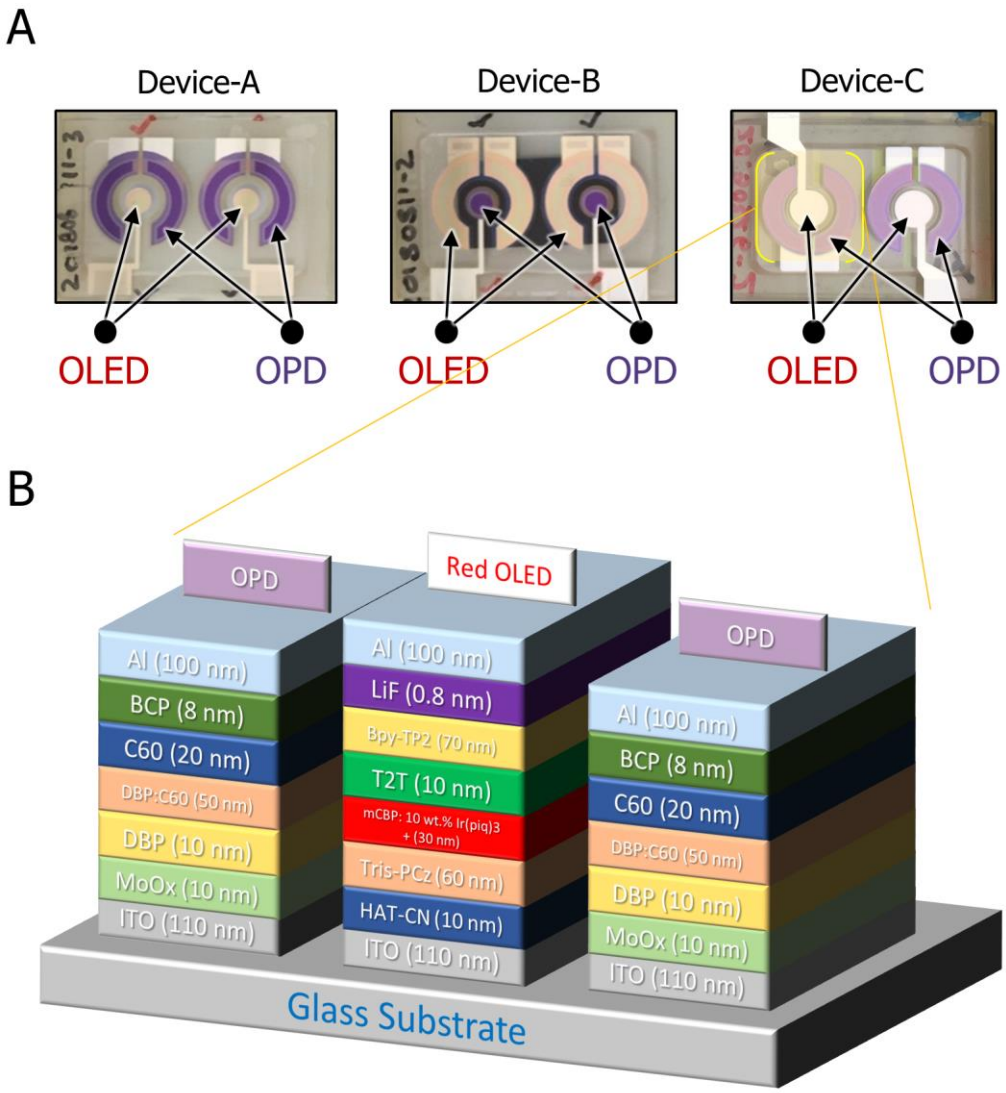

Figure 3.3: (**A**) The fabricated organic biosensor pulse meter for Device-A, Device-B, and Device-C. (**B**) A cross-section of the organic material structure of the OLED and OPD for all devices.

The performance of the OLED device is essential to the quality of the pulse meter measurements. The same material structures of the OLED/OPD were used in Device-A, Device-B, and Device-C. The fabrication process of the organic pulse meter sensor started with the preparation of 2.5 cm × 2.5 cm glass substrates that were coated with indium-tin-oxide (ITO) and cleaned via sonication in detergent, deionized (DI) water, acetone, and isopropyl alcohol (IPA). Next, the substrates were boiled in IPA for 10 minutes and subjected to UV-ozone treatment for 15 minutes. Then, the samples were loaded into an evaporator chamber where the organic and metal layers were deposited with proper shadow mask patterns for the OLED, followed by the OPD. The shadow masks were designed in a way to prevent the issue of misalignment in the multi-mask processing of monolithic device fabrication. After the evaporation processes, the samples were encapsulated without exposure to air in a glove box by glass lids using UV curable epoxy resin. Thereafter, the samples were used for evaluating the performance of the pulse meter sensor. Figure 3.3B illustrates the structure of the OLED and OPD used in Device-A, Device-B, and Device-C. The OLED device structure consisted of ITO (110 nm), a transparent anode that allowed the generated light to be emitted from the glass panel, HAT-CN (10 nm) as the hole injection layer, Tris-PCz (60 nm) as the hole transport layer, mCBP:10 wt.% $Ir(piq)_3$ + (30 nm) as the emissive layer where the holes and electrons recombined to emit light, T2T (10 nm) as the electron blocking layer, Bpy-TP2 (70 nm) as the electron transport layer, LiF (0.8 nm) as the electron injection layer, and Al (100 nm) as the cathode for the OLED.

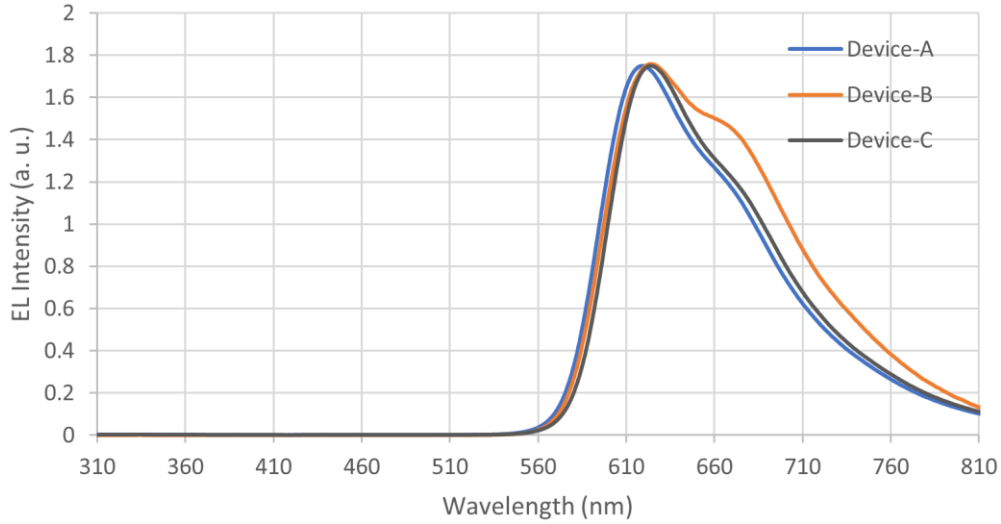

Figure 3.4: The OLED's electroluminescence spectrum with respect to the wavelength (nm).

The current density-voltage (JV)-luminance characteristics were evaluated using a Keithley 2400 source meter and an absolute external quantum efficiency (EQE) measurement system (C9920-12, Hamamatsu Photonics, Japan). The OLED was mounted to the entrance port of the measurement system's integrating sphere to collect the photons emitted from the front face of the devices. Each electroluminescence (EL) spectrum was collected by an optical fiber connected to a spectrometer (PMA-12, Hamamatsu Photonics). All measurements were performed in the ambient atmosphere at room temperature. The emission spectra in Figure 3.4 shows the EL characteristic of the OLED with respect to the wavelength, where the maximum intensity of light is at 625 nm. The slight difference in the EL spectrum of devices was due to the micro-cavity effects with different doping ratio or thickness variation where the devices were not fabricated at the same time.

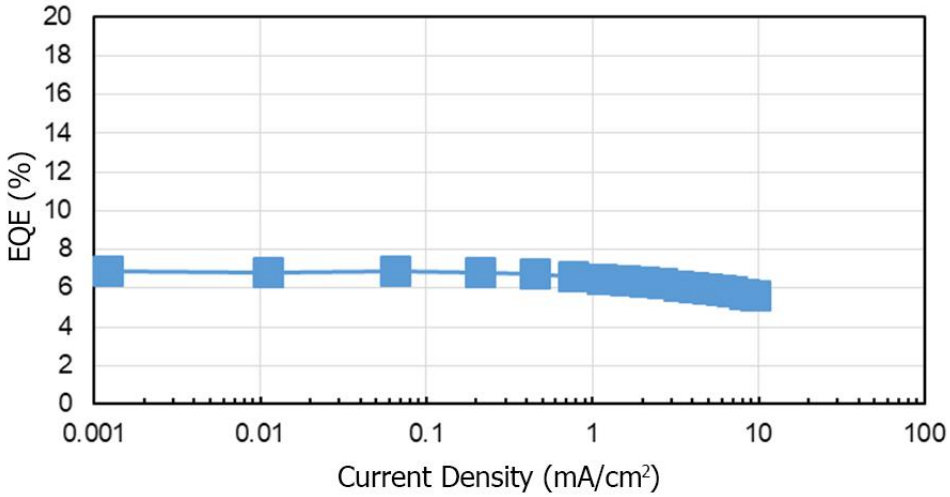

Figure 3.5: EQE of the OLED with respect to the current density (mA/cm^2).

Figure 3.5 shows the EQE with respect to the current density (mA/cm^2) where OLED device showed a low level of leakage current. The EQE of the OLED was measured about 7% at 1 mA/cm^{-2} current density. The current density in Figure 3.6 indicates a good OLED characteristic of, approximately, 10 mA/cm^2 at 5V. Eventually, we have been able to improve the OLED characteristics where the OLED host dopant ratio in the emissive layer and the thickness of hole/injection transport and injection layers were optimized in order to achieve high OLED EQE.

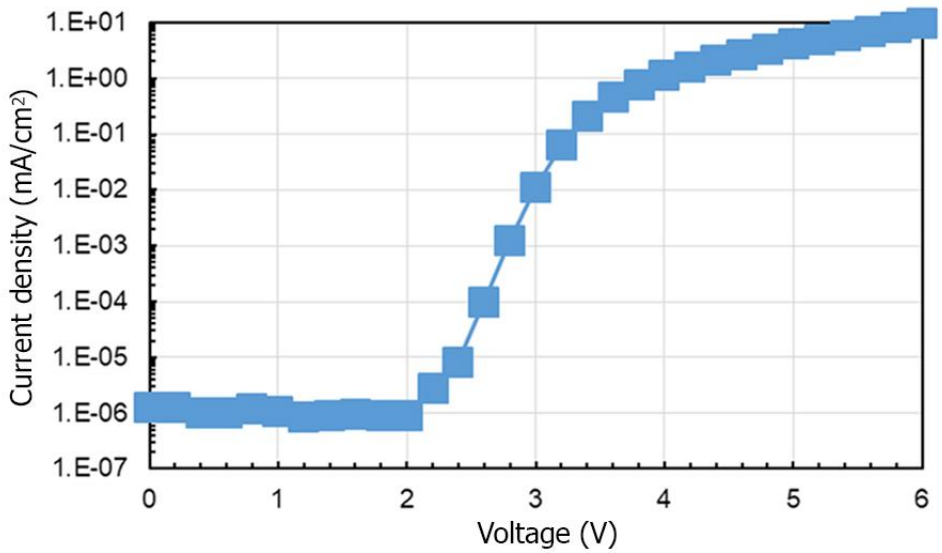

Figure 3.6: The current density (mA/cm^2) of the OLED with respect to voltage.

3.3.2 OPD Characterization

Measuring the amount of the reflected light from the skin layers and blood vessels on the large area of the OPD, compared to the PD, gives a better and stronger signal due to the high-detectivity of the OPD on a large detective area. As a result, the pulse meter device gives a better diagnosis of the PPG signal of the patient's condition. In the detecting circuit, we used no bias for the OPD sensor, which is a special characteristic of OPD over the silicon photodiode. The OPD structure consisted of ITO (110 nm), with MoO_x (10 nm) as the hole injection layer, DBP (10 nm), DBP:C60 (50 nm), and C60 (20 nm) combined in the device active layer, BCP (8 nm) as the electron transport layer, and Al (100 nm) as the cathode, as shown in Figure 3.3B.

The EQE spectra were collected using Bunkoukeiki SM-250GDP spectral response measurement system. The EQE of the OPD device at 625 nm, of a zero-bias condition for all devices, was about 37%, which overlapped with the EL spectrum of the red OLED wavelength, as shown in Figure 3.7. The slight difference in the characteristics of Device-A, Device-B, and Device-C was due to difference doping ratio or thickness variation because the devices were not fabricated at the same time.

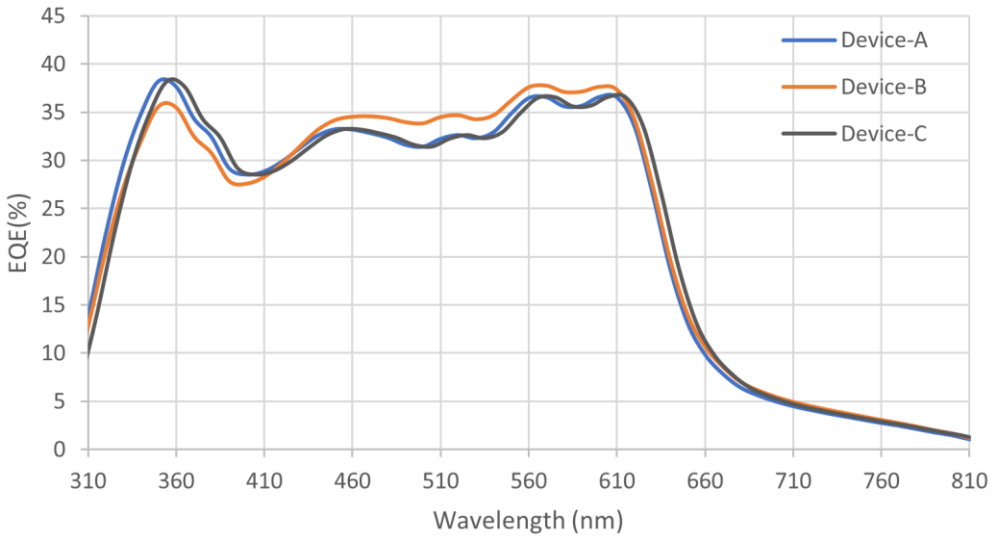

Figure 3.7: The OPD's external quantum efficiency (EQE) with respect to the wavelength for Device-A, Device-B, and Device-C.

The OPD can be fabricated to cover more wavelength spectrum, but in this work, we selected the DBP and C60 device structure because we were using red OLED and this OPD device configuration gave the best performance in the OLED wavelength region. In the case of fabricating a NIR OPD, the materials that used to fabricate the device are unstable, and it is difficult to synthesize low bandgap material that is required for NIR OPD device.

Eventually, the OPD characteristics have been improved. The donor/acceptor ratio and the buffer layer thickness have been optimized. In addition, the charge blocking/injection layers were improved to reduce the reverse dark current density of vacuum processed DBP:C60 and enhance the EQE of the OPD.

3.4 SUMMARY

As a summary, this chapter has discussed the results of the optical simulation that lead to the best design structure in terms of power consumption and signal quality. Additionally, it elaborated the proposed design structure of the organic optoelectronic pulse meter, fabrication, and characteristics of the optoelectronic devices.

CHAPTER FOUR:

THE SYSTEM DESIGN

4.1 INTRODUCTION

The system structure of the proposed pulse meter is composed of three parts: optoelectronic devices, an analog circuit, and a microcontroller unit (MCU), as illustrated in Figure 4.1.

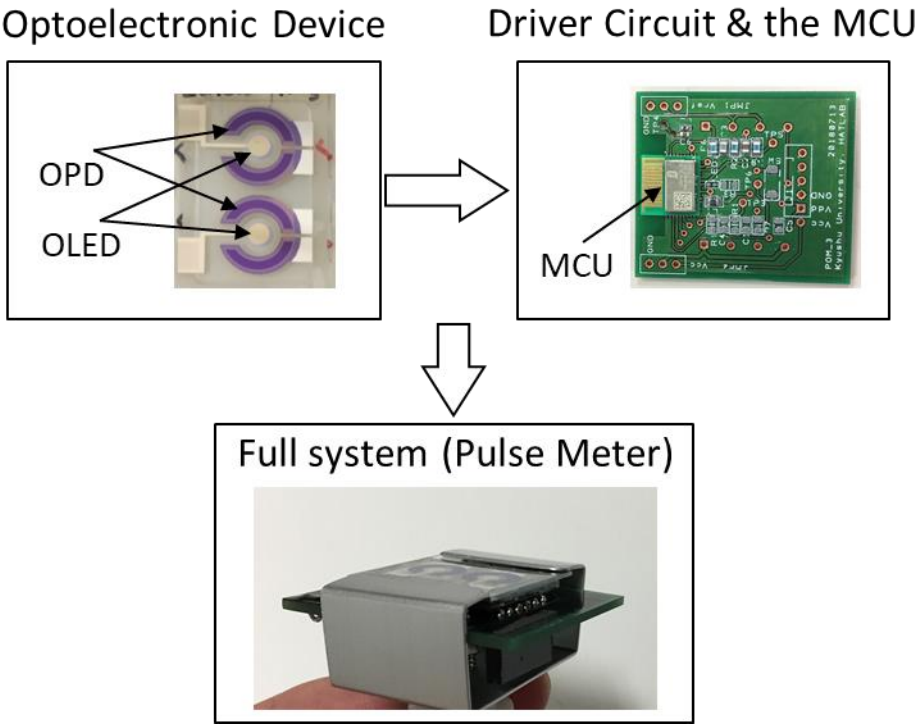

Figure 4.1: The system structure of the PPG detector device.

4.2 THE DRIVER CIRCUIT

There are different circuit topologies used for PPG acquisition systems such as the open-source schematic diagram shown in Figure 4.2, the Sallen-Key filter topology in Figure 4.3, and the multiple feedback (MFB) filter topology as shown in Figure 4.4.

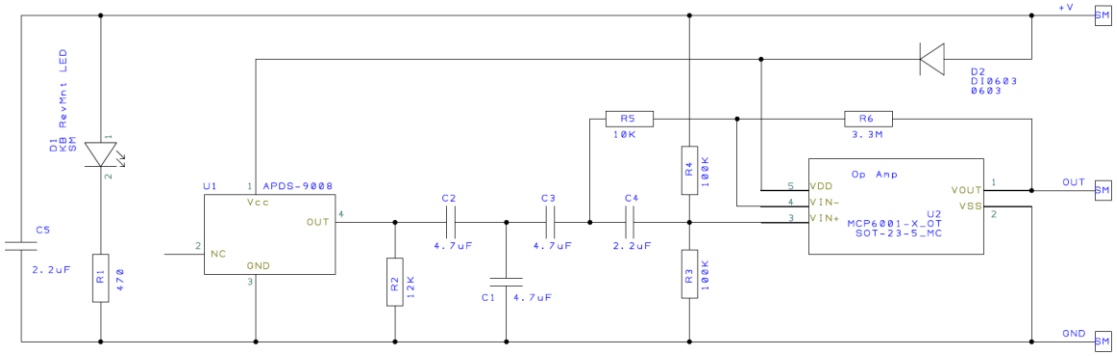

Figure 4.2: An open-source schematic diagram for the pulse sensor [53].

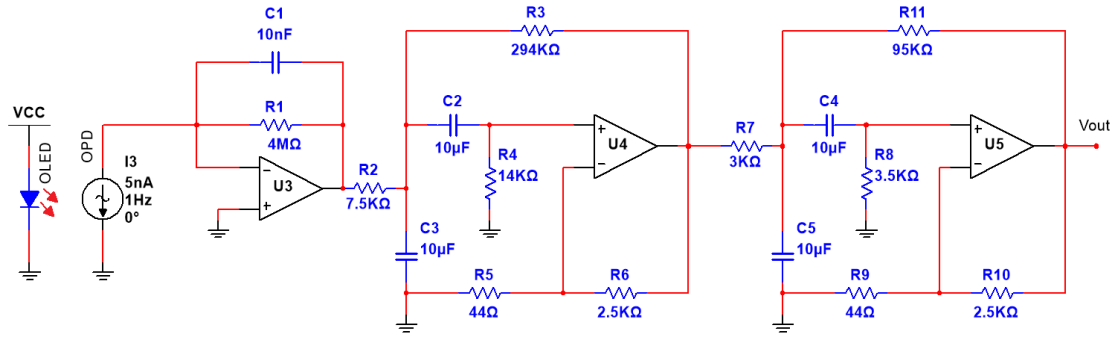

Figure 4.3: Two stages 2nd order bandpass filter (BPF) of Sallen-Key filter topology.

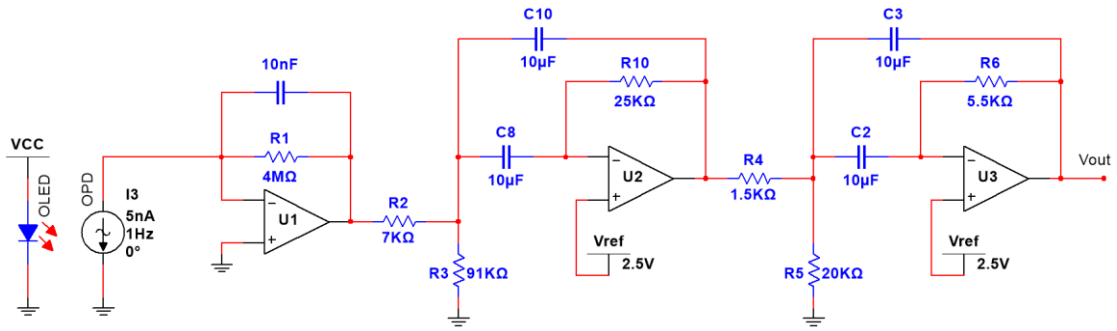

Figure 4.4: Two stages 2nd order BPF of multiple feedback (MFB) filter topologies.

The readout circuit in Figure 4.2, which is an open-source circuit for a commercialized pulse sensor, contains a miniature surface-mount (MSM) ambient light photosensor (APDS-9008, Broadcom Inc., San Jose, CA, USA) which includes a PD and operational amplifier (op-amp) inside the chip, as shown in Figure 4.5. This MSM ambient light photosensor outputs a voltage PPG signal which needs to be amplified

and filtered out from the noise in the following bandpass filter (BPF) of the circuit. V_{IN+} is connected with the voltage reference (V_{ref}), which is equal to $V_{dd}/2$. C4 is connected with the V_{ref} in order to minimize the noise to the lowest level by taking advantage of the common-mode rejection ratio (CMRR) of the op-amp. With this configuration circuit, the output PPG signal will be differentiated and amplified between 0 to V_{dd} volt, which is suitable for LED and PD pulse oximeter. However, this configuration circuit is not proper for OLED and OPD pulse oximeter, where the OPD generates current instead of voltage. Therefore, a transimpedance stage is needed in order to convert the current signal into a voltage signal.

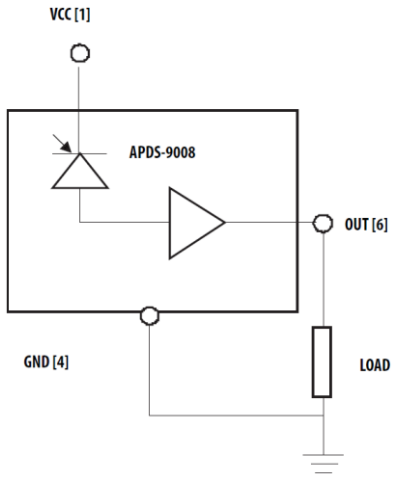

Figure 4.5: Typical application circuit for APDS-9008, [54]

In Figure 4.3, a pulse oximeter schematic diagram consists of TIA stage and two stages 2nd order bandpass filter (BPF) of Sallen-Key filter topology with a high gain. The first stage is necessary and effective, while the second stages of BPF are challenging where the op-amps must be a dual supplied in order to amplify the positive and negative signals. Whereas in the single supply op-amp, it will only amplify the positive signal which is not suitable for our circuit. Moreover, the circuit contains three

active components and 16 passive components, which indicates more power will be consumed, and many components will be packed in a small size PCB, which may affect the output signal. On the other hand, the circuit diagram in Figure 4.4 consists of TIA stage and two stages of 2nd order BPF of multiple feedback (MFB) filter topologies. It overcomes the limitation of amplifying the negative signal by connecting a V_{ref} on the V_{IN+} of the op-amp in order to shift the negative signal to the positive level. However, the circuit has a limitation on the gain. When the gain increases, the Q-factor increases as well and results in not flat magnitude response in the passband, which will cause an unstable output signal, as shown in Figure 4.6.

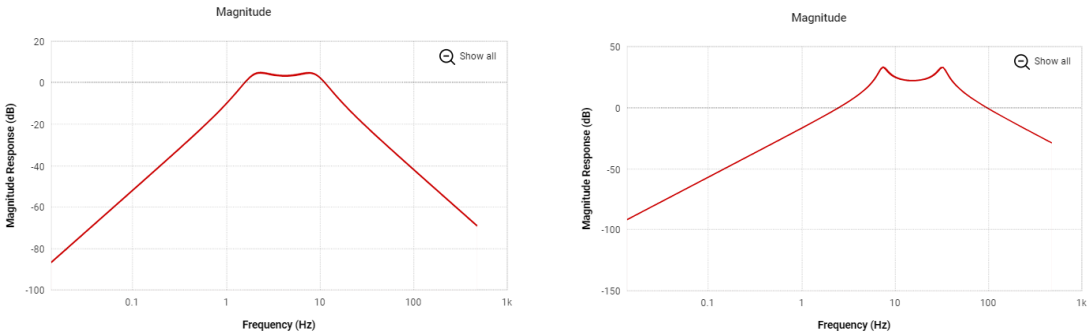

Figure 4.6: Bode Plots of two stages, 2nd order BPF, of MFB filter topology at; (A) 10 dB gain; (B) 50 dB gain.

Eventually, in order to miniaturize the PCB size and reduce the power consumption in the circuit while maintaining the best performance for the pulse meter, we chose to reduce the passive components and simplify the driving circuit into three main stages; transimpedance stage, filtration stage, and amplification stage, as shown in Figure 4.7.

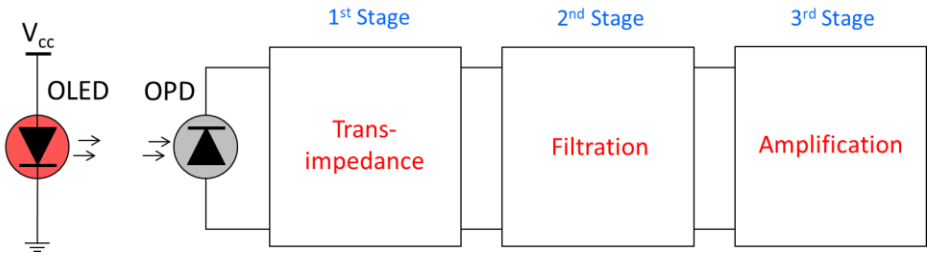

Figure 4.7: The pulse meter's driver circuit structure stages.

The generated photocurrent by the OPD, as a response of the reflected light from the blood vessels, is a very small amount in the nano ampere range, which requires a current-to-voltage converter such as a transimpedance amplifier (TIA) to convert the OPD output current to a voltage signal in the first stage of the analog circuit. The next stage is the analog filtration process where the PPG signal needs to be filtered out before the amplification. The last stage after filtering the signal is to amplify it to be suitable for the analog-to-digital converter (ADC) process in order to send the data via a serial communication block (SCB) or Bluetooth low energy (BLE) using the MCU. These stages are discussed in more details in the following sections.

4.2.1 Transimpedance Stage

Transimpedance amplifier (TIA) is a current-to-voltage converter that used to translate the current output of OPD to a voltage signal, which is an essential stage that needs to be done. It is used with a sensor that has a current response that is more linear than the voltage response. The TIA should have a low input impedance and low output impedance to avoid impedance mismatch in the circuit. It offers low impedance to the OPD and isolates it from the output voltage of the operational amplifier, [55,56]. Hence, it converts the low-level current of a sensor to a voltage, which is a necessary stage that needs to be done. Figure 4.8 illustrates a basic TIA circuit we applied for a single supply op-amp.

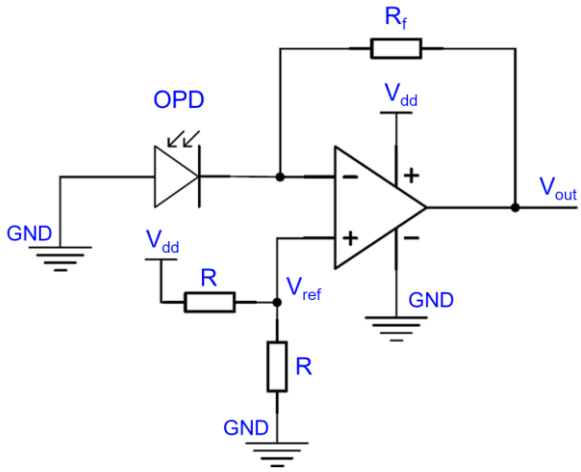

Figure 4.8: Basic transimpedance amplifier (TIA) circuit for a single supply.

$$V_{out} = -iR_f + V_{ref} \qquad \text{Equation 4.1}$$

4.2.2 Filtration Stage

The PPG signal contains an alternating current (AC) component and a direct current (DC) component. The AC component of the pulse signal is the small variations caused by the changing in the reflected light intensity because of blood flow into and out of the finger, while The DC component represents the total reflected light on the photosensor. In the filtration process we need to eliminate the DC component and amplify the AC component because if we were to amplify the raw signal without filtration, the DC part of the signal would saturate the amplifier before getting the desired amplification of the AC (time-varying) part. Consequently, to eliminate the DC signal and to improve the signal-to-noise ratio (SNR), a bandpass filter that composed of low pass filter (LPF) and high pass filter (HPF) is applied at a lower cut-off frequency (f_L) 0.5 Hz and a higher cut-off frequency (f_H) 16 Hz while attenuating any signals outside of these two frequencies. The LPF is applied to eliminate the high-frequency noise coming from the ambient light fixture and appliances at 60 Hz and 120 Hz. It is worthwhile to mention that choosing a very low cut-off frequency will cause

information loss in the PPG signal such as the systolic peak, dicrotic notch, and diastolic peak. On the other hand, the HPF is applied to eliminate the DC signal which is a very low-frequency signal coming from the DC component of the PPG signal in order to be able to amplify the AC component to the desired amplitude.

The first part of the band-pass filter, low pass filter, can be implemented with one capacitor in parallel with the feedback resistance, Figure 4.9, with a cut-off frequency (f_c) shown in Equation 4.2. However, these two filters, HPF and LPF, can be combined to one operational amplifier to create a band pass filter. Therefore, RC values should be chosen to fit the pass-band frequencies and gains.

$$f_c = \frac{1}{2\pi R_1 C_1}$$ Equation 4.2

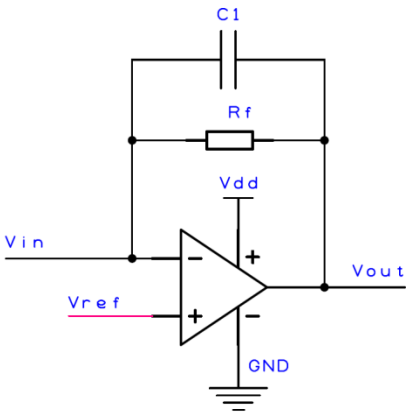

Figure 4.9: Block diagram of an active low pass filter.

The second part of the band-pass filter can be implemented with a capacitor in series with the input resistance, which creates a high-pass filter, as shown in Figure 4.10. The cut-off frequency (f_c) and the voltage gain are as shown in Equation 4.3 and Equation 4.4:

$$f_c = \frac{1}{2\pi R_1 C_1}$$ Equation 4.3

$$A_V = -\frac{R_f}{R_1}$$ Equation 4.4

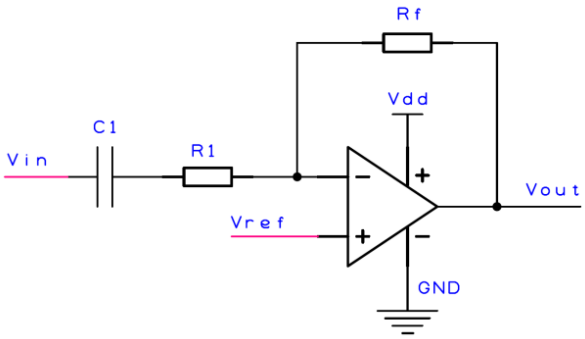

Figure 4.10: Block diagram of an active high pass filter, which acts as a differentiator.

4.2.3 Amplification Stage

An inverting operational amplifier, Figure 4.11, is a good option to be selected for amplifying the PPG signal as it is common to be used in a single supply design. This amplifier can output the signal amplitude near to the V_{dd} power supply. The signal must be amplified in the range of 0 to V_{dd} instead of centered around 0V. A virtual ground (V_{ref}) needs to be engaged to accomplish this by amplifying the changes with respect to the (V_{dd}/2) volts.

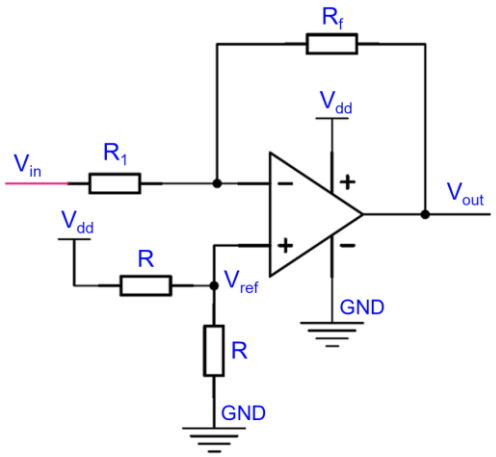

Figure 4.11: Block diagram of an inverting operational amplifier.

By combining these three stages we will be able to get the first differentiation PPG signal, Figure 4.12, from the readout circuit. To increase the PPG signal quality, the order of the filter should be increased. Therefore, a feedback capacitor C_3 was added to the amplification stage for increasing the LPF order to the 2nd order which improved the PPG signal as shown in Figure 4.13. In the 2nd order filter, the stop band roll-off will be twice the 1st order filter at −40 dB/decade as the frequency increases above the cut-off frequency. Figure 4.14 shows the simplified readout circuit for acquiring the PPG signal from the pulse meter where the aim is to reduce the passive components for miniaturizing the PCB area, and to reduce the power consumption and maintain the best performance for wearable pulse meters.

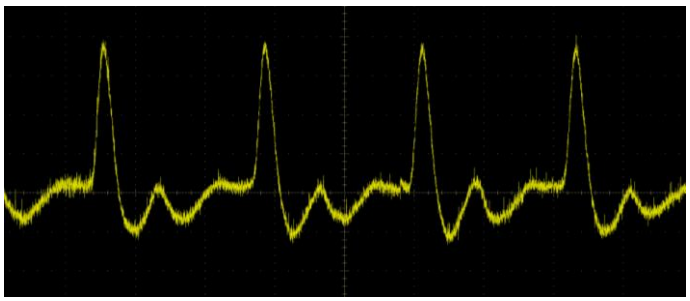

Figure 4.12: A differentiation PPG signal from the 1st order LPF filter.

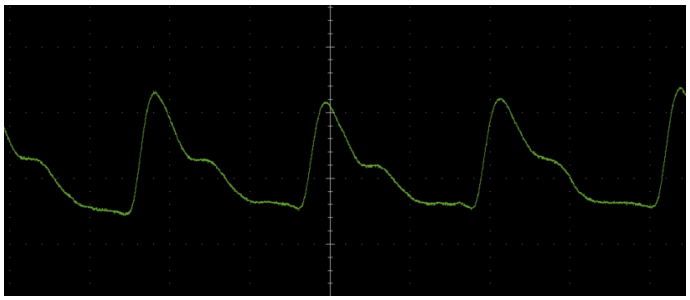

Figure 4.13: A PPG signal from the 2nd order LPF filter.

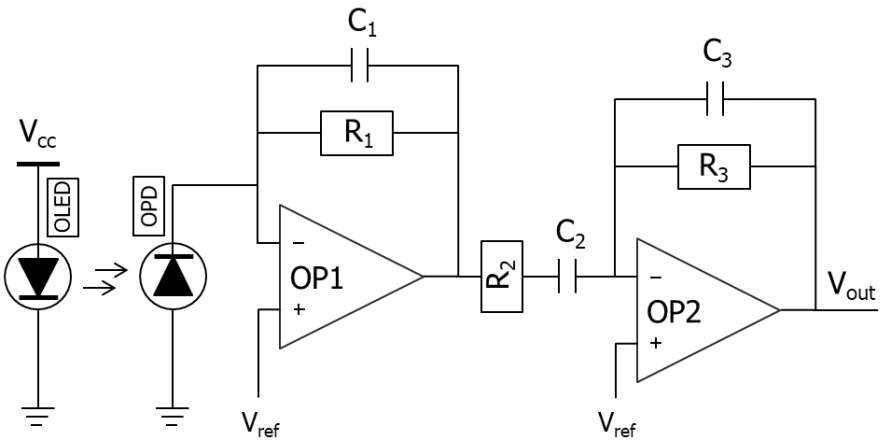

Figure 4.14: The simplified analog circuit for acquiring the PPG signal from the pulse meter.

The final output comes from two stages op-amps, the output from the first stage is named as V_1, which is described as follow;

$$V_1 = A_{OL}(V_+ - V_-) \quad \text{Equation 4.5}$$

V_+ is connected to the Vref;

$$V_1 = A_{OL}(V_{ref} - V_-) \quad \text{Equation 4.6}$$

V_- is a function of both V_1 and the voltage on the Z1;

$$V_1 = A_{OL}(V_{ref} - (iZ_1 + V_1)) \quad \text{Equation 4.7}$$

$$V_1 = A_{OL}V_{ref} - A_{OL}iZ_1 - A_{OL}V_1 \quad \text{Equation 4.8}$$

$$V_1 = \frac{A_{OL}V_{ref} - A_{OL}iZ_1}{1 + A_{OL}} \quad \text{Equation 4.9}$$

and since the A_{OL} is very large, the equation can be simplified to;

$$V_1 = -iZ_1 + V_{ref} \quad \text{Equation 4.10}$$

$$i = i_{DC} + i_{AC} \quad \text{Equation 4.11}$$

$$Z_1 = R_1 // \left(\frac{1}{SC_1}\right) = \frac{R_1}{1 + SC_1R_1} \quad \text{Equation 4.12}$$

where, $S = jw$

$$V_1 = -i\left(\frac{R_1}{1 + SC_1R_1}\right) + V_{ref}$$ Equation 4.13

at stage 2, the output is equal to;

$$\frac{V_1 - V_{ref}}{Z_2} = \frac{V_{ref} - V_{out}}{Z_3}$$ Equation 4.14

$$\frac{V_{out}}{Z_3} = \left[\frac{V_{ref}}{Z_3} - \frac{V_1 - V_{ref}}{Z_2}\right]$$ Equation 4.15

$$V_{out} = -\left(\frac{Z_3}{Z_2}\right) \cdot V_1 + \left(\frac{Z_3}{Z_2} + 1\right) \cdot V_{ref}$$ Equation 4.16

$$V_{out} = -\left(\frac{Z_3}{Z_2}\right) \cdot \left(-iZ_1 + V_{ref}\right) + \left(\frac{Z_3}{Z_2} + 1\right) \cdot V_{ref}$$ Equation 4.17

$$V_{out} = \left(\frac{Z_3}{Z_2}\right) \cdot Z_1.i - \left(\frac{Z_3}{Z_2}\right) \cdot V_{ref} + \left(\frac{Z_3}{Z_2}\right) \cdot V_{ref} + V_{ref}$$ Equation 4.18

$$V_{out} = \left(\frac{Z_3}{Z_2}\right) \cdot Z_1.i + V_{ref}$$ Equation 4.19

$$Z_1 = \frac{R_1}{(1+SC_1R_1)}, \quad Z_2 = R_2 + \frac{1}{SC_2}, \quad Z_3 = \frac{R_3}{(1+SC_3R_3)}$$
$$,\left(\frac{Z_3}{Z_2}\right) = \frac{\frac{R_3}{(1+SC_3R_3)}}{R_2+\frac{1}{SC_2}} = \frac{SC_2R_3}{(1+SC_3R_3)(1+SC_2R_2)}$$ Equation 4.20

$$V_{out} = \frac{SC_2R_1R_3}{(1 + SC_1R_1)(1 + SC_2R_2)(1 + SC_3R_3)} \cdot i + V_{ref}$$ Equation 4.21

Therefore, the transfer function (TF) of the driver circuit including the BPF and the amplification is stated in Equation 4.22, which indicates three negative poles of a stable system where we can simulate the frequency response of the circuit.

$$H(S) = \frac{SC_2R_1R_3}{(1 + SC_1R_1)(1 + SC_2R_2)(1 + SC_3R_3)}$$ Equation 4.22

4.2.4 SPICE Simulation

The analog circuit for detecting the PPG signal was simulated on Multisim software. A capture of the schematic circuit is shown in Figure 4.15. The circuit consists

of two op-amps, two constant current sources, several resistors, and capacitors. The bypass capacitors, C4 and C5, were added to filter the high frequency from the power source that goes to the chip and the circuit. They connected in parallel to reduce the equivalent series resistor (ESR) and the equivalent series inductors (ESL). A capacitor can be connected with an op-amp to the ground in order to prevent it from oscillating and making noise. The constant current I3 from the subcircuit_1 is added to cancel the DC current of the OPD in order to amplify the AC current without saturation in the TIA stage.

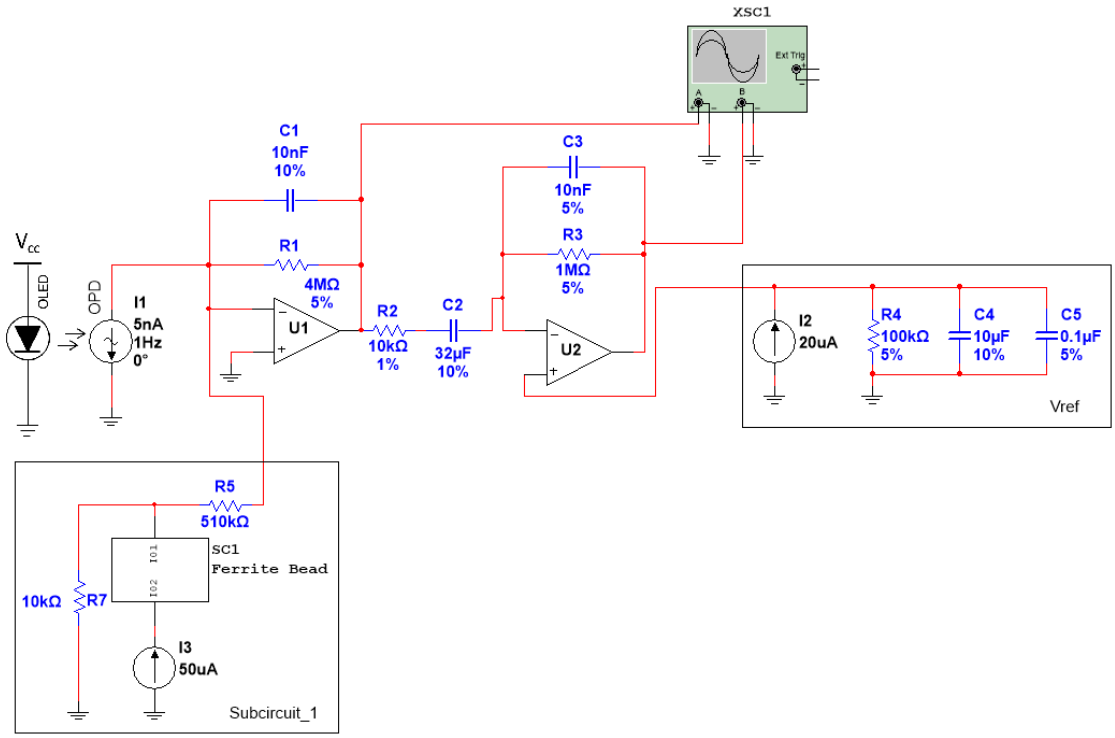

Figure 4.15: The analog circuit for detecting the PPG signal that simulated on Multisim.

The circuit was designed as a second-order LPF and a first-order HPF which in combined are making a BPF. The filters' cut-off frequencies are analyzed in the following equations;

$$LPF\ (1), f_H = \frac{1}{2\pi R_1 C_1} = \frac{1}{2\pi(4M)(10n)} = 3.98\ Hz$$ Equation 4.23

$$LPF\ (2), f_H = \frac{1}{2\pi R_3 C_3} = \frac{1}{2\pi(1M)(10n)} = 15.9\ Hz$$ Equation 4.24

$$HPF, f_L = \frac{1}{2\pi R_2 C_2} = \frac{1}{2\pi(10K)(32\mu)} = 0.49\ Hz$$ Equation 4.25

The AC sweep simulation of the output signal at the second op-amp "Vout_2" is shown in Figure 4.16 which shows the Bode Plot of the bandpass filter circuit, whereas the amplitude simulation of the output at the first and second op-amp is shown in Figure 4.17.

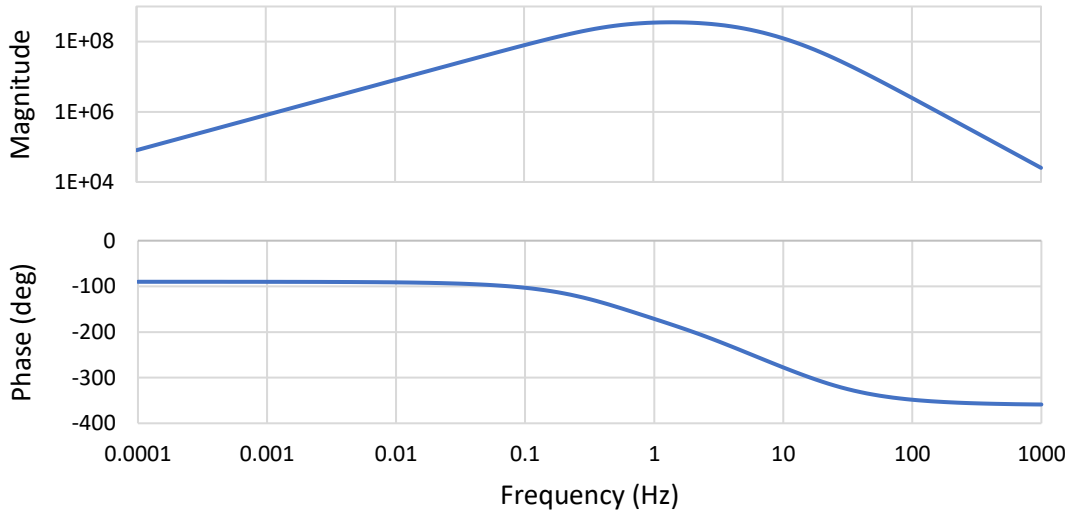

Figure 4.16: The Bode plot of the bandpass filter circuit.

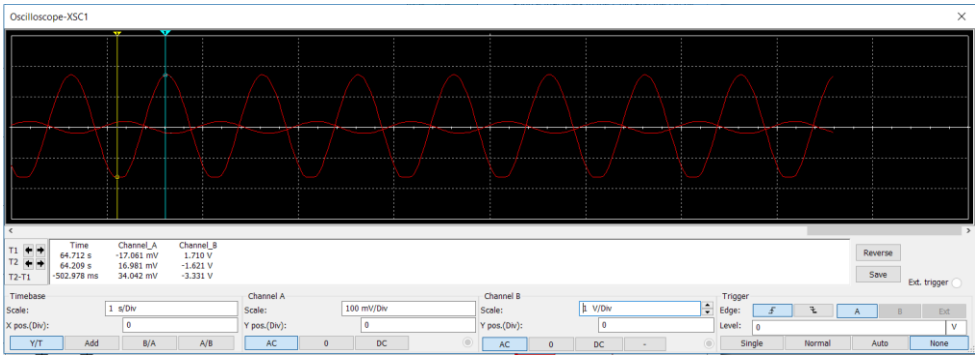

Figure 4.17: Amplitude simulation of the circuit from "Vout_1" at "Channel_A" and "Vout_2" at "Channel_B".

The schematic diagram and the PCB circuit for the pulse meter device were designed using (DesignSpark PCB 8.1, USA) software. A capture of the schematic circuit is shown in Figure 4.18. Also, the capture of the PCB circuit is shown in Figure 4.19.

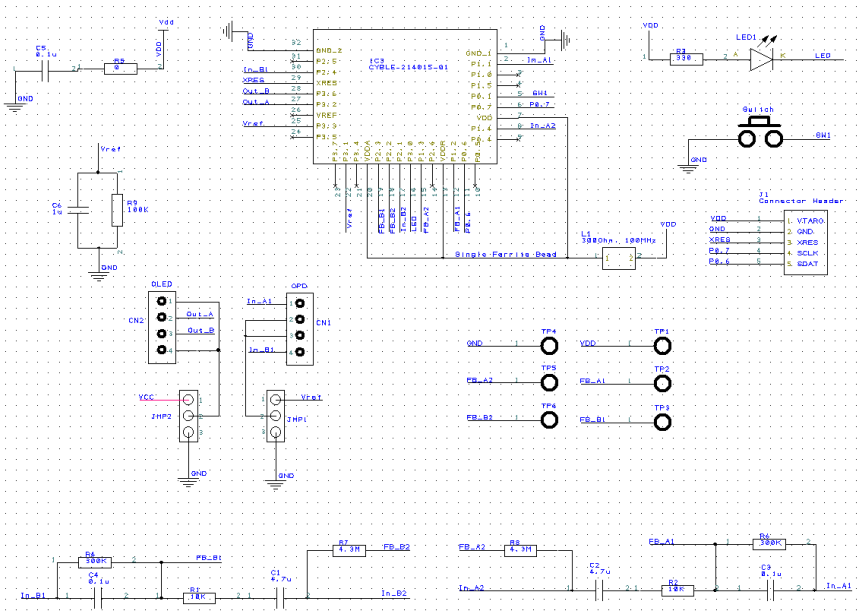

Figure 4.18: The schematic diagram of the PCB circuit.

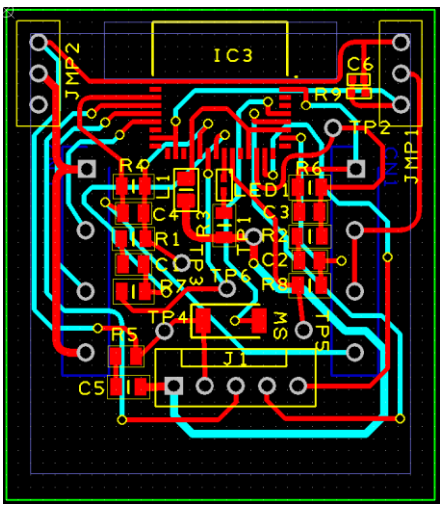

Figure 4.19: The PCB circuit diagram of the pulse meter.

The BLE chip, PSoC 4, was programmed using (PSoC Creator 4.2, Cypress, USA) software. A capture of the schematic circuit is shown in Figure 4.20.

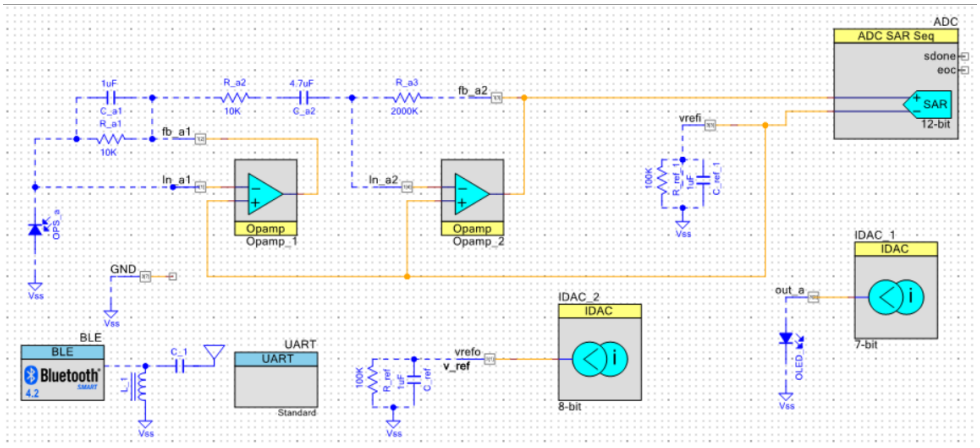

Figure 4.20: The schematic diagram of PSoC Creator program.

4.2.5 Microcontroller Unit

Bluetooth low energy (BLE) is a protocol for wireless communication over short distances using short-wavelength UHF radio waves from 2.4 to 2.485 GHz and building point-to-point (P2P) topology for one-to-one device communications between the central and the peripheral. It optimizes data transfers with very low power consumption [57]. BLE improves battery life by offering low-power modes, during which the chip offers restricted performance or features, with the benefit of much lower power consumption while in those modes. The Microcontroller Unit (MCU) module that we applied in this work is PSoC 4 BLE chip (Cypress Semiconductor, San Jose, CA, USA), which is a certified and qualified chip supporting BLE wireless communication. This module offers five low-power modes (Active, Sleep, Deep-Sleep, Hibernate, and Stop mode) to optimize the design for the lowest possible power consumption. In its Active mode, the CPU current consumption is 1.63 mA (at 3 MHz), while it is 1.03 mA (at 3 MHz) in Sleep mode. In its Deep-Sleep mode, the power consumption is only 1.3 µA while maintaining the BLE Link-Layer active. The Hibernate mode consumes 150 nA, while the Stop mode consumes the minimum power consumption, 60 nA, when the

device is on complete standby. In our application, the chip switches between these modes at a certain time for better performance and saving power consumption.

We configured the BLE's generic attribute (GATT) as a server and the generic access profile (GAP) as a peripheral. GAP's roles are to define who is central and who is peripheral, and it has a responsibility of establishing and maintaining the connection. GATT supervises the server and the client communication relationship. In the GAP settings, the advertising interval selected as a fast advertising interval with a minimum 20 ms, and the minimum connection interval 7.5 ms to 50 ms. The logical link control and adaptation layer protocol (L2CAP) logical channel are set as 1 channel and L2CAP MTU size is 23 bytes. The security level selected as unauthenticated pairing with encryption for easier connection between the central and the peripheral. The encryption key size is 16 bytes. The ADC of the PPG signal is set at 166666 sample per second (SPS) with actual clock frequency 4000kHz and a resolution of 8 bits. The input range of the ADC is selected from voltage reference value 3.3 V to V_{ss} 0 V.

BLE sends the data as a data packet at a very short time, close to a few milliseconds. Figure 4.21 illustrates the structure of the link-layer protocol data unit (PDU) packet, which describes the one data packet. The preamble is a 1-byte value that applied for timing and synchronization estimation at the receiver. Its address is always as 0xAA for broadcasted packets. The access address is also fixed for broadcasted packets. The link-layer payload consists of a header, channel ID, and attributes a maximum transmission unit (ATT_MTU). The header defines the packet type and describes the function of the device. Cyclic redundancy check (CRC) is the final part of the transmitted packet, which is an error-detecting code that used to confirm the packet for unwanted changes [58].

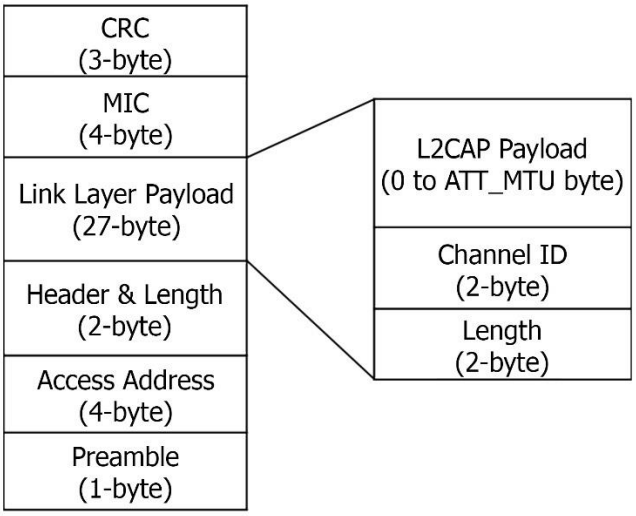

Figure 4.21: BLE 4.1 link layer PDU structure [59].

In order to ensure the capability of the BLE module to our application, we examined the real measured maximum payload throughput of two BLE modules connection, ver.1, and ver.2. The maximum throughput was measured using the PSoC Creator program from [59] on the BLE module and displayed on terminal window software (Tera Term, Ver. 4.93).

After connecting and configuring the dongle with the desktop to receive the data from the BLE wirelessly, the first module (CYBLE-022001-00) was able to send 2 kbps at the minimum connection interval 7.5 ms, as shown in Figure 4.22. Whereas the maximum payload throughput from the second module (CYBLE-214015-01) was 256 kbps, which is optimum for our application at a low frequency applied (0.5 Hz to 16 Hz). The income data is displayed on a terminal window, TeraTerm software, using a universal asynchronous receiver-transmitter (UART) component, as shown in Figure 4.23.

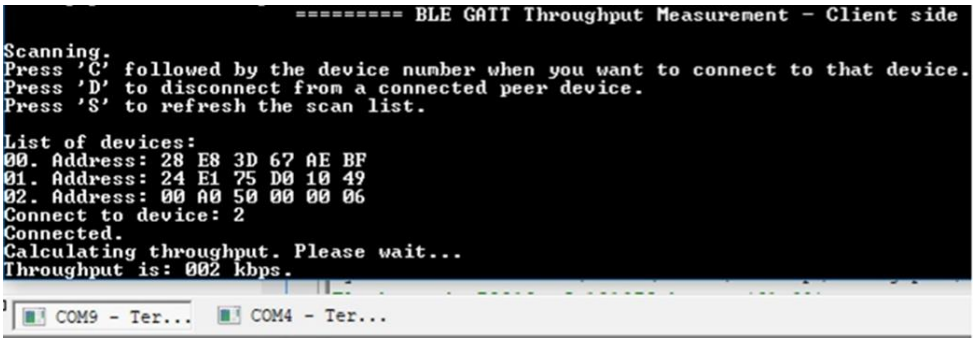

Figure 4.22: The real measured payload throughput of the BLE module Ver.1 (CYBLE-022001-00).

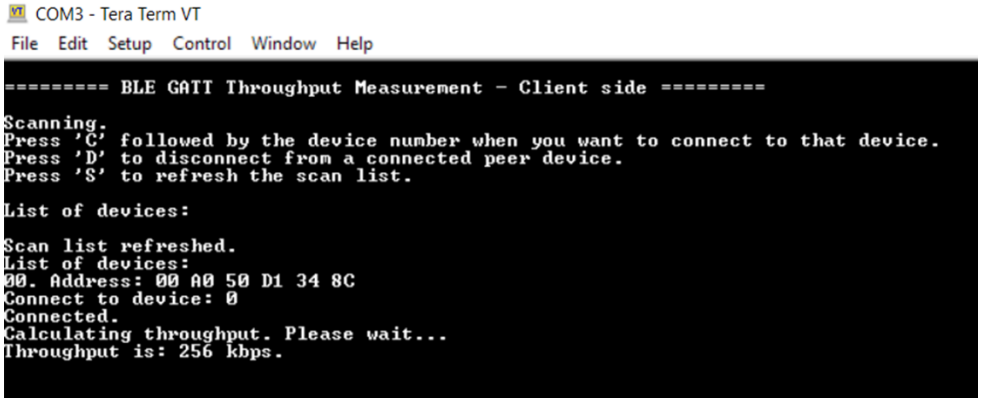

Figure 4.23: The real measured payload throughput of the BLE module Ver.2 (CYBLE-214015-01).

4.2.6 Mechanical Part

The proposed pulse meter has three main parts; the PCB, the optoelectronic devices, and the holder. The PCB part included the drive circuit and the MCU, whereas the optoelectronic devices included the OLED and the OPD device. An innovative pulse meter holder was proposed to fix all the parts together tightly in an easy way in order to prevent any movements of the OLED/OPD device, as shown in Figure 4.24. When the screw is tightened, the PCB goes up and push the glass substrate up by the spring-loaded connector. As a result, all parts will be fixed safely. The aluminum metal was used in the holder to eliminate the static and ambient noise.

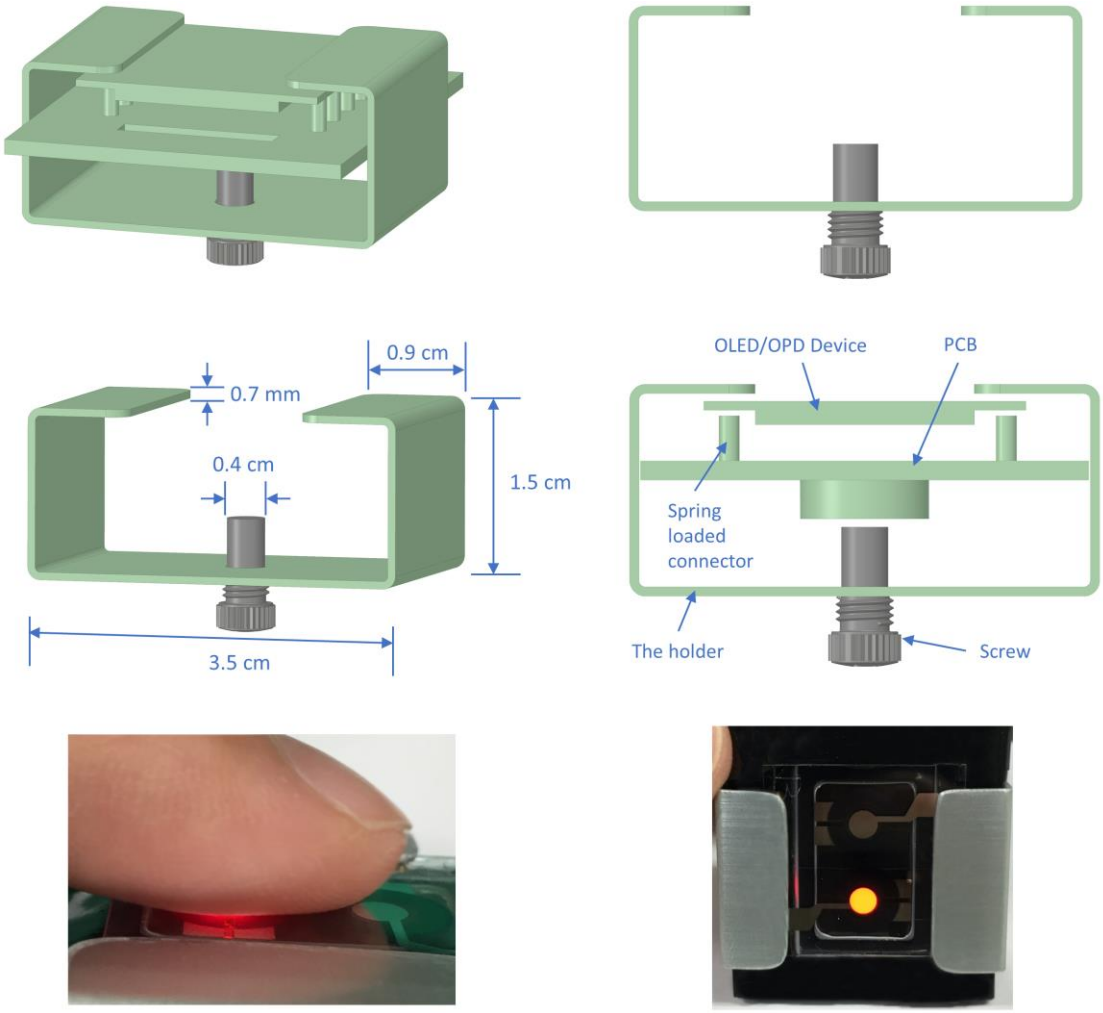

Figure 4.24: The illustration and dimensions of the proposed pulse meter holder that used to fix the parts together.

4.3 DIGITAL FILTER

In portable pulse meters, the PPG signals are susceptible to corruption by noise and motion artifacts, where the analog filter is not adequate to eliminate these noises. Hence, the digital filter was implemented to improve the PPG signal's quality. There are several noise reduction methods using digital signal processing techniques in the literature such as the discrete wavelet transform (DWT) [40], morphological characteristics comparison [42], and cluster analysis [43]. However, it is difficult to implement these methods into embedded systems due to their requirements and complexity. Therefore, we implemented a finite impulse response (FIR) digital filter in

order to improve the signal's quality. The representative equation of the FIR digital filter is shown in Equation 4.26 and Equation 4.27:

$$y[n] = \sum_{k=0}^{L} b_k \, x[n-k] \qquad \text{Equation 4.26}$$

$$b[k] = \begin{cases} \alpha + (1-\alpha)\cos\left(\frac{2\pi k}{N}\right) & -N \le k \le N \\ 0 & elsewhere \end{cases} \qquad \text{Equation 4.27}$$

where $y[n]$ is the output sequence of the digital filter; $x[k]$ is the input sequence; L is the interval; $b[k]$ is the weight coefficient; and α is the Hamming window coefficient 0.54, [60,61]. The cut-off frequency of the FIR digital filter was set at 16 Hz, as choosing a very low cut-off frequency would alter the PPG waveform structure and lose information from the signal such as the systolic peak, dicrotic notch, and diastolic peak, as shown in Figure 4.25. The FIR digital filter reduced the noise and enhanced the stopband slope from −20 dB/decade in the analog filter to more than −80 dB/decade.

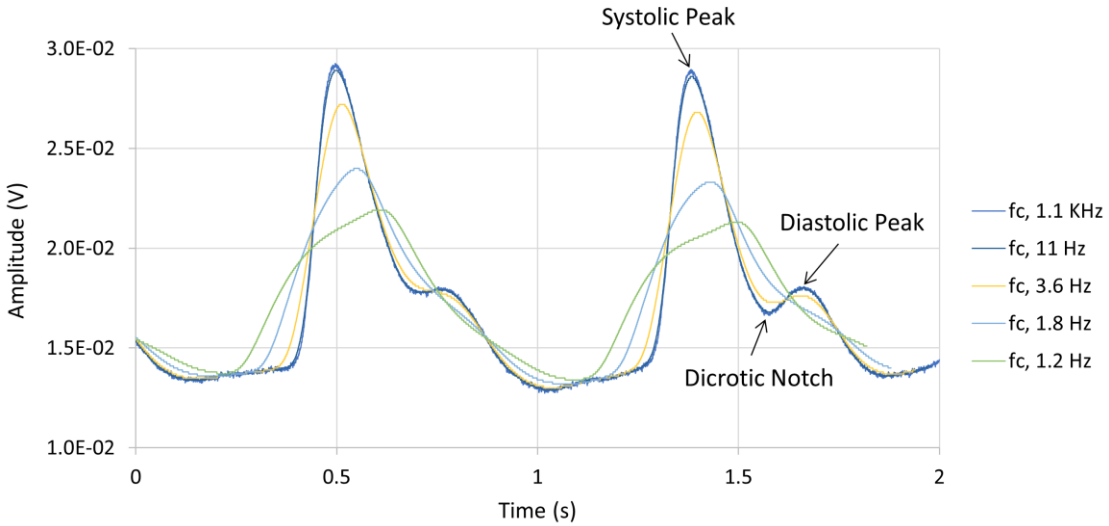

Figure 4.25: Digital low-pass filter effect on the PPG signal, where the signal lost its morphological structure if the cut-off frequency (f_c) was set very close to the carrier frequency.

4.4 SNR MEASUREMENT

The common term for quantifying the digital signal is the signal-to-noise ratio (SNR), and it can be simply calculated, as formulated in Equation 4.28. Fast Fourier transform (FFT) is a fast computation algorithm for discrete Fourier transform (DFT), which is defined by the formula in Equation 4.29. FFT analysis was used to compute the noise of the digital signal by converting the time-domain signal to the frequency domain by decomposing a sequence of values into components of different frequencies.

$$SNR_{dB} = 20log_{10}\left(\frac{A_{signal}}{A_{noise}}\right) \qquad \text{Equation 4.28}$$

where A_{signal} is the amplitude of the signal and A_{noise} is the amplitude of the noise.

$$X_k = \sum_{n=0}^{N-1} x_n \, e^{-i2\pi kn/N}, \qquad k = 0, \ldots, N-1 \qquad \text{Equation 4.29}$$

where x_n is a discrete-time input sequence; X_k is the DFT, and N is the number of samples.

The spectra of the FFT is a series of $N/2$ points in the frequency domain from 0 Hz to $f_s/2$ Hz, where N is the number of samples, and f_s is the sampling frequency. The SNR of the PPG signal is calculated by subtracting the amplitude of the PPG signal from the amplitude of the noise level in dB, as illustrated in Figure 4.26.

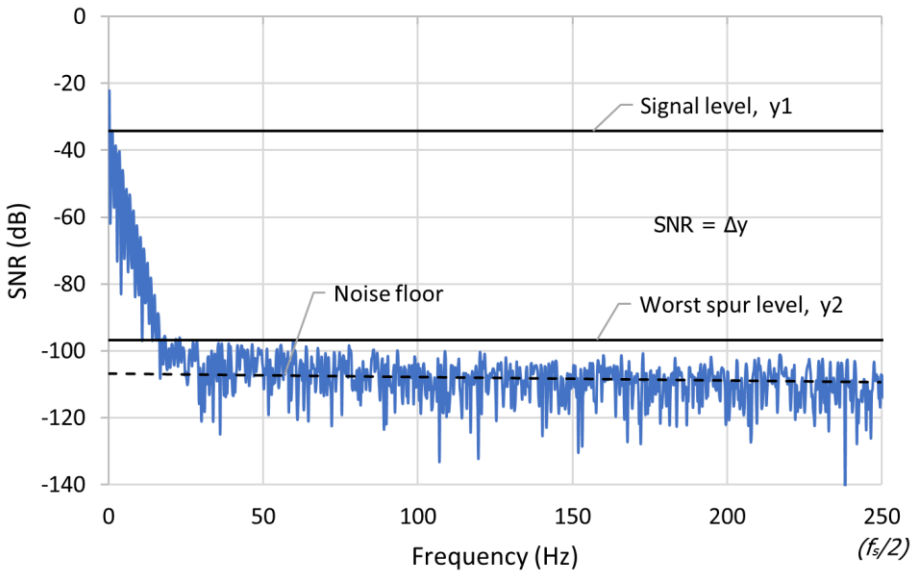

Figure 4.26: Fast Fourier transform waveform to calculate the signal-to-noise ratio (SNR) of the PPG signal.

4.5 PULSE RATES MEASUREMENT

There are several methods in the literature to detect the peaks of the PPG signal in order to calculate the HR. Some researchers used complicated signal processing methods such as PPG peak detection based on multi-scale data analysis using Empirical Mode Decomposition (EMD) [62] or using wavelet-based cascaded adaptive filter as in [63] and [64], while other researchers proposed adaptive detection using different ways, for instance, in [65] they proposed an adaptive threshold detection for PPG signals where a pre-defined slope parameter was decided to find V_{max} and V_{min} using MATLAB software which is not proper for real-time embedded systems. In [66] an adaptive segmentation method was proposed for detecting the peaks of the PPG signals. It starts by segmenting the PPG signal into several segments and detecting the peak values in each segment. Then, the peak values were compared to decide if the segment slope has a negative or positive slope, where the peak of a PPG pulse determined as the peak of a positive segment that followed by a negative segment. However, this method has a limitation in the noisy signals especially if a small curvy noise has existed in the signal

then it will be detected as a peak, and it also cannot decide the slope of two peaks with the same value. To overcome that limitation, we proposed another approach for detecting the PPG signal based on an adaptive threshold and segmentation method. The algorithm is summarized in the following steps:

Step 1: For the first 2 seconds (T_s), find the V_{max} and V_{min} of the PPG signal and calculate the peak-to-peak amplitude ($V_{p\text{-}p}$).

Step 2: Make a segment every ($T_p \times (1/k)$) second and find the max and the min value for each segment, where T_p is the time interval between two peaks which has an initial value of 1 and k is the number of segments.

Step 3: Select any discrete point its value equal to $\{V_{p\text{-}p} \pm 20\%\ V_{p\text{-}p}\}$ as a max peak segment (S_{p1}) and any value less than $\{V_{p\text{-}p} - 80\%\ V_{p\text{-}p}\}$ as a min trough segment (S_{t1}).

Step 4: Take the max value among the three neighbor values $\{S_{p1}, S_{p2}, S_{p3}\}$ if existed, and that value is the first peak P_1.

Step 5: Take the min value among three neighbor values $\{S_{t1}, S_{t2}, S_{t3}\}$, and that value is the first trough T_1.

Step 6: Update $V_{p\text{-}p}$ value based on P_1 and T_1 values.

Step 7: Update T_p which is equal to $\{T_p = | T_{P(t)} - T_{P(t-1)} |\}$.

Step 8: Calculate the pulse rate, $PR_1 = 60 / T_p$.

Step 9: Update the pulse rate average (PRA) by adding the $(PR_1 + PR_2 \ldots PR_n)/n$ for 60sec, then start to update the PRA from the beginning, as shown in the flowchart in Figure 4.27.

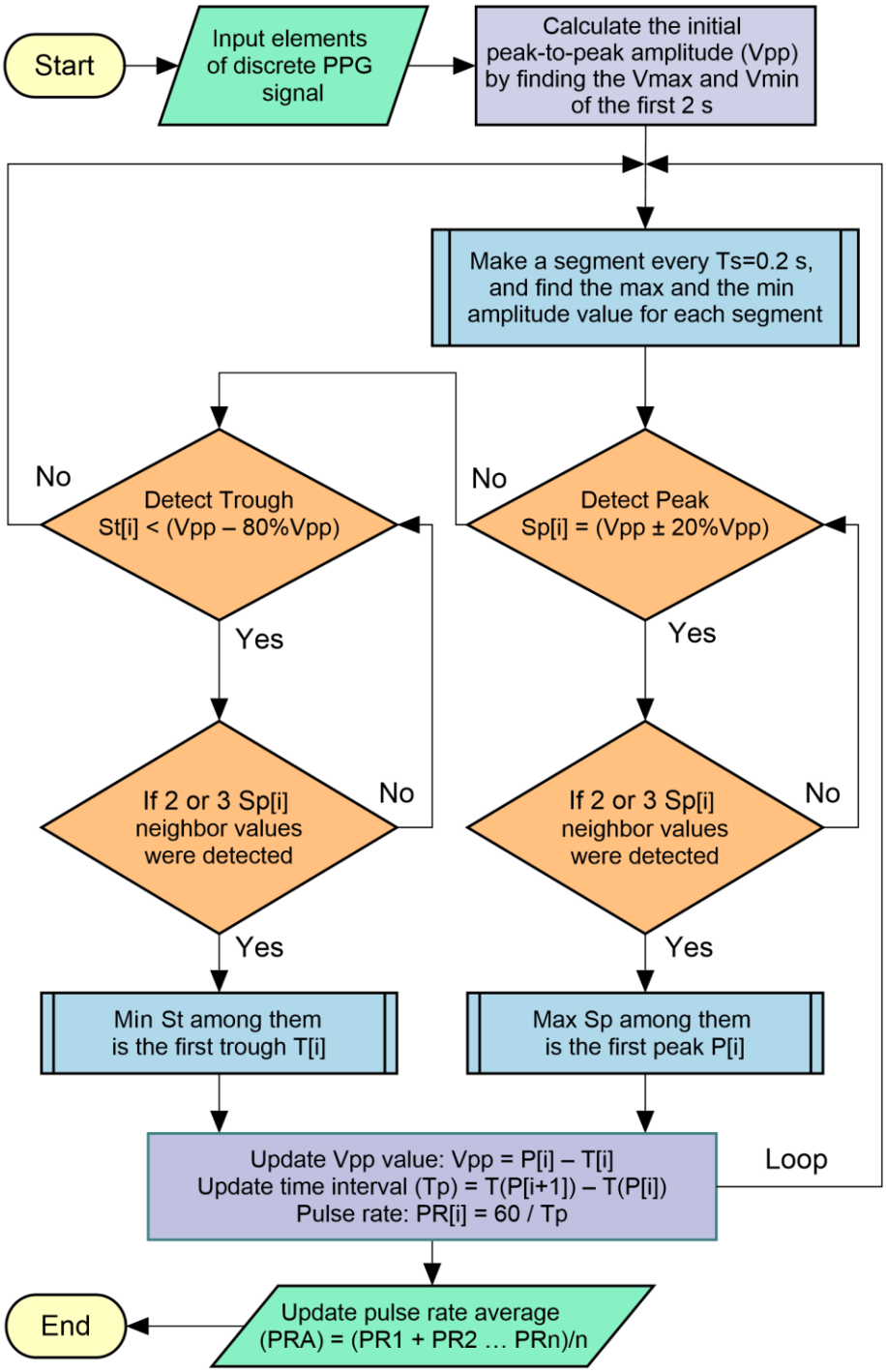

Figure 4.27: The algorithm flowchart for estimating the pulse rate average (PRA).

Accordingly, the proposed method demonstrated to be suitable for our application by achieving high overall accuracy (1.5) percent error of the heart rate compared to the commercially reference we obtained.

4.6 SUMMARY

This chapter has elaborated the system design that developed for the proposed organic pulse meter. The detecting circuit, including its stages, the SPICE simulation, the MCU, and the mechanical parts of the pulse meter were explained thoroughly. The MCU module that we applied in this work was the PSoC4 CYBLE-214015-01 module, and it was compared with the previous module in terms of payload throughput. The BLE PSoC4 improved the battery life by offering low-power modes, during which the chip offered restricted performance for the lowest possible power consumption. Moreover, it illustrated the digital filter design that was applied to the system, the approach of measuring the SNR, and the algorithm for estimating the pulse rates.

CHAPTER FIVE:

RESULTS AND DISCUSSIONS

5.1 INTRODUCTION

The obtained PPG signal from the pulse meter device needs to be quantified in order to estimate the device reliability. This section discusses the results of the comparison between Device-A, Device-B, and Device-C and the results of the PPG signal on several parts of the body. The proposed devices were tested on healthy individuals who gave informed consent before participating in the study.

5.2 COMPARATIVE RESULTS FOR DEVICE-A AND DEVICE-B

The performance of the proposed pulse meter was tested in vivo on a healthy male subject. The portable pulse meter was attached to the index finger to acquire the PPG signal from Device-A and Device-B sequentially, to compare their performance. The PPG signals were obtained from the same subject for a specific time period while he was resting in a chair. For the evaluation process, the data were recorded at the sampling frequency of 500 SPS. The FIR digital filter was applied at a 16 Hz cut-off frequency. The heart rates were extracted accurately in both devices and estimated by averaging the beat-to-beat interval of the peaks in the PPG signal. The portable pulse oximeter (NURSE ANGIE, Custom Co., Tokyo, Japan) was selected as a reference device for estimating the pulse rate (PR) due to its ability to measure the PR in the range of 25 bpm to 250 bpm with a resolution of 1 bpm and accuracy of 3% error. The proposed pulse meter showed accurate results of about 1.5% error of the PR compared to the commercial reference. Figure 5.1 shows the comparison between the PPG waveform of

Device-A and Device-B before and after applying the digital filter. Both devices were reliable and acquired the PPG signal clearly and were almost similar in their outputs.

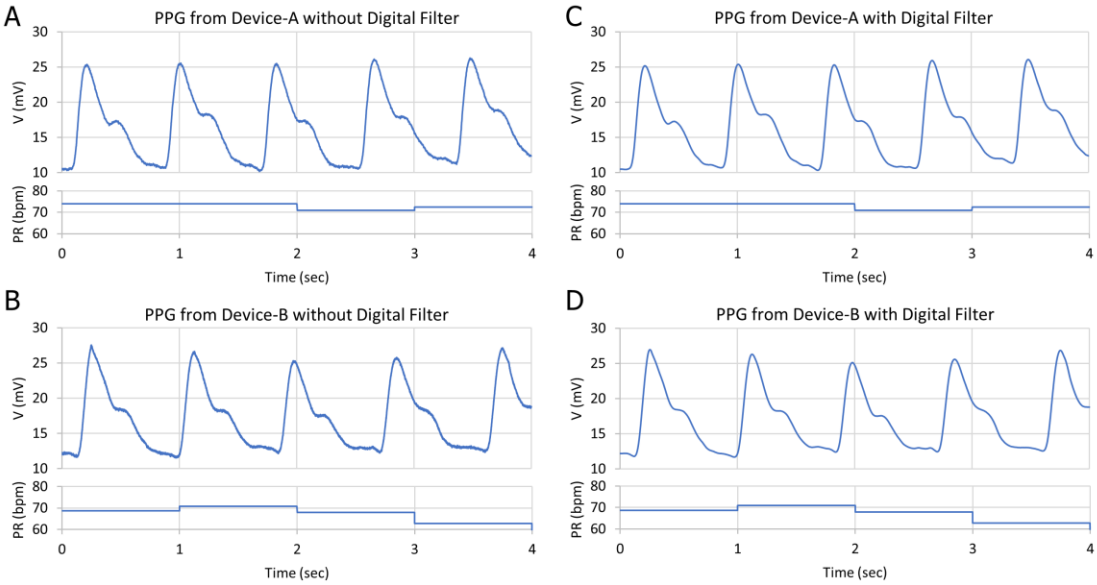

Figure 5.1: Comparison between the PPG signal from; (**A**) Device-A without a digital filter; (**B**) Device-B without a digital filter; (**C**) Device-A after applying a digital filter; and (**D**) Device-B after applying a digital filter.

A summary of the PPG signal characteristics of Device-A and Device-B are shown in Table 5.1.

Table 5.1: Summary of the PPG signal's quality for Device-A and Device-B.

Sample No.	**Average Vp-p (mV)**	**SNR (dB) without Digital Filter**	**SNR (dB) with Digital Filter**	**Current Consumption (μA)**	**Power Consumption (mW)**
Device-A	15	45.4	62.6	20	0.1
Device-B	14.5	47.4	63.3	1600	8

The amplitude $V_{p\text{-}p}$ of the PPG signal in Device-A and Device-B was roughly 15 mV, which was as expected in the optical simulation where the amount of reflected light that was received from both OPDs was almost equal. There was a slight difference between the SNR in Device-A and Device-B, which could be due to the difference in

the OPD dimension area where the biggest area gained more noise. It is noteworthy that the power consumption recorded a significant disparity between the two devices, where Device-B consumed 8 mW, while Device-A consumed only 0.1 mW. Consequently, these findings support the assumption that designing an OLED to emit a large amount of light is not necessary to produce a high-quality PPG signal; instead, it will consume more power. On the other hand, designing an effective OLED and OPD structure guided by optical simulation led to the best results in terms of power consumption and signal quality. The digital filter demonstrated a noticeable improvement of about 25% in both devices from 45.4 dB to 62.6 dB in Device-A and from 47.4 dB to 63.3 dB in Device-B. As a result, Device-A was selected as the effective device structure in terms of power consumption and quality level in comparison with Device-B.

5.2.1 Results of Device-A on Different Body Parts

The Device-A pulse meter was attached to multiple locations on the body (index finger, middle finger, little finger, forearm, wrist, and forehead) within a specific time period. The PPG signals were obtained from those body locations sequentially, from the same subject, in order to compare the PPG signal quality between them, as shown in Figure 5.2. Device-A successfully showed a very clear PPG signal on the fingers and a lower quality signal on the forearm, wrist, and forehead. Table 5.2 summarizes the amplitude, the average pulse rate (PR), and the SNR of the different PPG signals.

The amplitude of the PPG signal varied between 2–20 mV in the devices. There are several factors that can affect changes in the signal amplitude and can be influenced by the type of human skin, the position of the finger on the OPD, and how much pressure is applied from the finger to the OPD where the amount of the reflected light from the arterial blood vessels on the OPD changes based on that pressure. The SNR table

demonstrated a very good quality level from the three fingers with an average of 56 dB and showed a good quality from the forehead of 51.4 dB, while it presented a lower quality signal on the forearm and on the wrist position of about 46 dB, as the fat tissue in these parts is thicker, and the arterial blood vessels are deeper than in the skin tissue. In such cases, the intensity of the OLED needs to be increased, which means more power is consumed. For that trade-off between the SNR level and power consumption, we chose a suitable current source for the OLED at 20 µA, 5 V, in order to obtain a very good quality signal from the fingers and a good quality signal from the other body parts. The PR was calculated accurately based on the algorithm discussed in Chapter 4. The results showed that the proposed pulse meter based on the new OLED and OPD design structure was capable of acquiring the PPG signals accurately and consistently at a low power consumption of 0.1 mW.

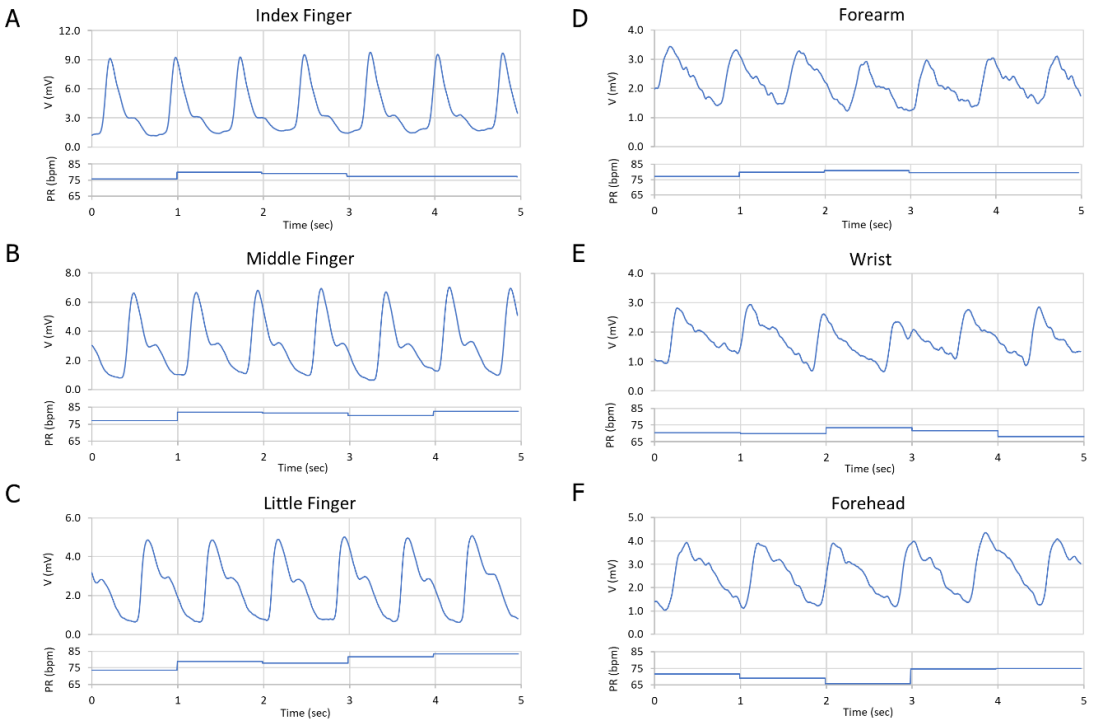

Figure 5.2: Comparison between the PPG signal on different parts of the body: (**A**) Index finger; (**B**) Middle finger; (**C**) Little finger; (**D**) The forearm; (**E**) The wrist; and (**F**) The forehead.

Table 5.2: Summary of the PPG signal's quality from different parts of the body.

Position name	V_{p-p} (mV)	SNR (dB)
Index finger	8.1	58.3
Middle finger	6.0	57.2
Little finger	4.2	54.4
The forehead	2.9	51.4
The forearm	2.0	46.9
The wrist	2.3	45.7

5.3 COMPARATIVE RESULTS FOR DEVICE-A AND DEVICE-C

Device-A and Device-C were evaluated in vivo on a healthy male subject, on his index finger. The PPG signal was collected from both devices sequentially, within a specific time period, while he was sitting on a chair. The data were recorded at the sampling frequency of 500 SPS, 8-bit resolution from the SCB and used to evaluate both devices. Figure 5.3 shows that both devices were reliable and obtained a clear and stable PPG signal. With Device-C, Figure 5.3A, the peak-to-peak amplitude (V_{pp}) of the PPG signal was about 100 mV, while in Figure 5.3B, the PPG amplitude of Device-A was less than 45 mV with a constant voltage of 5 V of the OLED. Consequently, the power consumption of each device was different. Device-A consumed about 0.6 mW and Device-C about 1.6 mW. Therefore, in order to unify the power consumption of both devices, we supplied a constant current. We compared the amplitude and signal-to-noise ratio (SNR) values of both devices for each PPG signal at different OLED's driving currents, from 1.2 μA to 93.6 μA, as shown in Figure 5.4. The constant current was supplied using the MCU's analog current source. Table 5.3 summarizes the PPG signal characteristics of Device-A and Device-C.

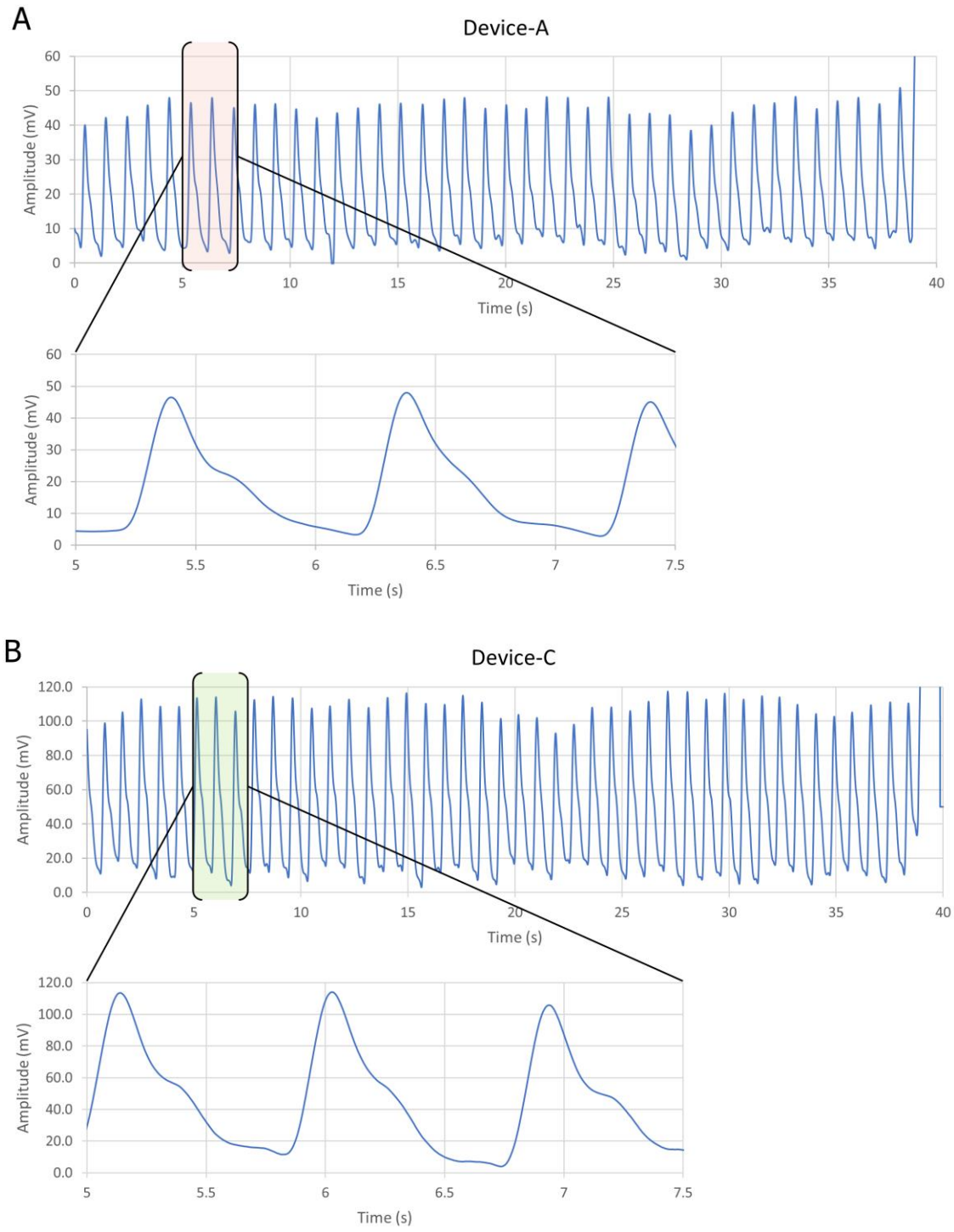

Figure 5.3: Obtaining the PPG signal from (**A**) Device-A at a constant voltage source and (**B**) Device-C at a constant voltage source.

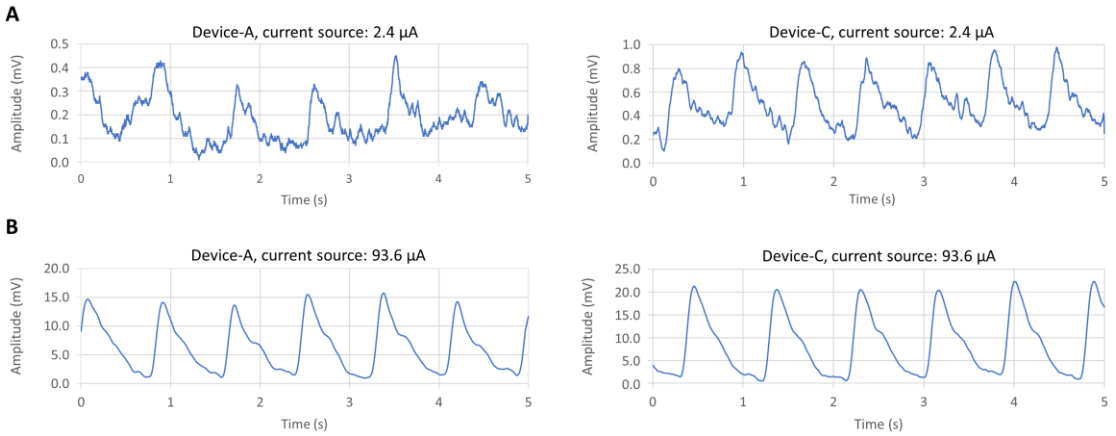

Figure 5.4: Comparison between the PPG signals from Device-A and Device-C at two different current sources for OLED; (**A**) at 2.4 µA and (**B**) at 93.6 µA.

Table 5.3: Summary of the PPG signal quality for Device-A and Device-C.

Device No.	Average Vp-p (mV)	SNR (dB)	Current Source (μA)
Device-A	13	46	93.6
Device-C	20	45	93.6
Device-A	0.3	8	2.4
Device-C	0.7	18	2.4

Figure 5.5 compares the SNR values from Device-A and Device-C of different gap distances at different current consumptions. It shows that decreasing the distance of the gap between the OLED and the OPD, in Device-C, leads to an increase in the DC noise on the OPD, as was indicated by the SNR results with respect to the OLED current. The SNR of Device-A at a higher OLED current of 93.6 µA was 46 dB, whereas it was 45 dB in Device-C at the same current source even though its PPG signal amplitude was smaller than Device-C. On the other hand, reducing the gap between the OLED and the OPD resulted in a higher SNR of the PPG signal at a lower OLED current. As shown in Table 5.3, the PPG signal amplitude increased from 0.3 mV at 8 dB in Device-A to 0.7 mV at 18 dB in Device-C, where the gap distances between the OLED and the OPD were 2 mm and 1.65 mm for Device-A and Device-C, respectively. It is worth mentioning that Device-C produced an acceptable PPG signal of about 18 dB with ultra-

low power consumption, as low as 8 µW. Consequently, from these results, Device-C demonstrated a significantly advantageous SNR at a low current supply compared to Device-A where the short gap between the OLED and the OPD increased the chance of obtaining more reflected light. That means the shorter gap between the OLED and the OPD devices will result in improving the SNR at the low power consumption, and the larger gap will result in reducing the SNR.

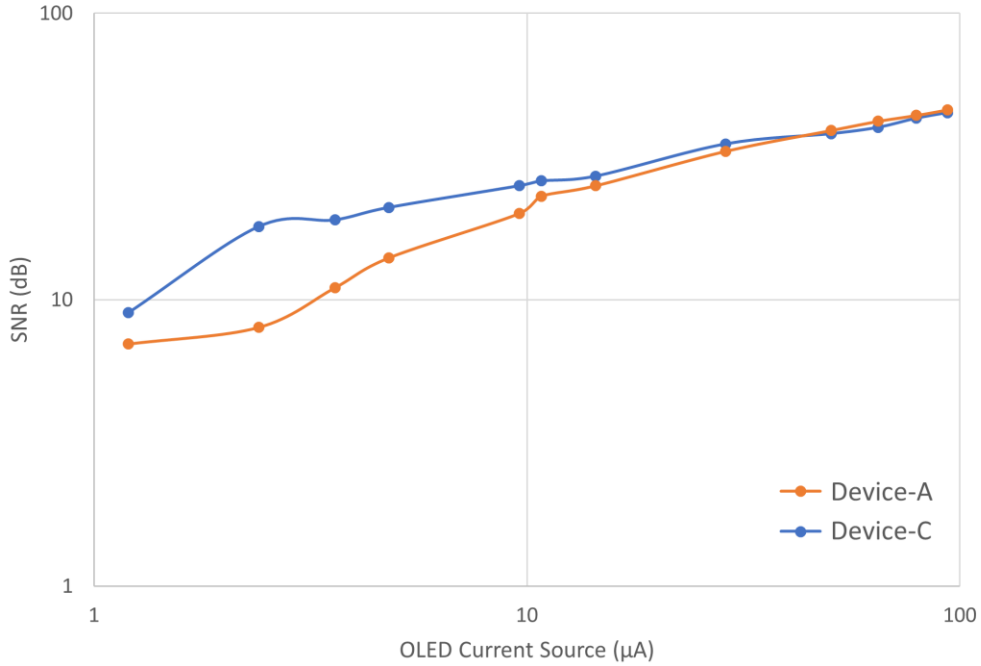

Figure 5.5: Comparison of the signal-to-noise ratio (SNR) of the PPG signals from Device-A and Device-C at different OLED driving currents from 1.2 µA to 93.6 µA.

Although the gap distance between the OLED and the OPD was a top priority while designing an organic pulse meter, another two aspects that should be taken into consideration are the OLED's area and OPD's area. For the OLED's area, if we reduced the OLED's area in order to reduce the power consumption, the OLED's lifetime will also be reduced because the current density will be increased on a small area. On the other hand, if the OLED's area increased, then the area in the center of the OLED will

be impractical and will not contribute to increasing the reflected light from the human body. For the OPD's area, it should be designed in a way to surround the OLED sufficiently in order to collect more reflected light. However, increasing the OPD's area too much will result in increasing the DC noise. Therefore, the area of the OPD should be consistent with OLED design, which can be achieved by optical simulation.

Table 5.4 compares the results between our device and other devices, despite the fact that the previous PPG signal monitoring systems are different than our current proposed device in terms of device characteristics, flexibility, and signal quality. The proposed device consumes the lowest power for light source among them.

Table 5.4: Comparison table between our device and other devices.

	This work (at low current)	**This work (at higher current)**	**Ref. [28]**	**Ref. [27]**	**Ref. [25]**
OLED Type	Red OLED	Red OLED	Red OLED	Red PLED	Red OLED
Device Flexibility	Rigid	Rigid	Flexible	Flexible	Rigid
Voltage Supply (V)	3.3	5	3.3	5	9
OLED Driving Current (μA)	2.4	20	21	1000	20000
OLED area (mm2)	6	3	0.5	N.C.	4
Power Consumption (μW)	8	100	24	N.C.	N.C.
PPG signal-to-noise ratio (dB)	18	45	N.C.	N.C.	N.C.

5.4 ACQUIRING PPG SIGNALS FROM BLE

This section presents the results of the wireless PPG waveforms from Device-C, which was selected as the more effective device, in terms of power consumption, for the portable pulse meter. The PPG signal was obtained from the index finger of the

subject while he was resting in a chair during a specific period of time. The data were obtained wirelessly from the portable organic pulse meter using BLE technology. The PPG signal was transmitted to a PC host using a universal serial bus (USB) dongle (PRoC BLE CYBL10162-56LQXI, Cypress Semiconductor, San Jose, CA, USA) with 500 SPS of ADC and 8-bit resolution. The recorded length of the PPG signal on the receiving PC host was constrained by the sampling rate of the ADC in the chip. Although the BLE chip had an on-air data rate of 1000 kbps, the maximum throughput data rate between the chip and the receiver PC host was 256 kbps at a minimum connection interval of 7.5 ms. The maximum throughput was measured using the PSoC Creator program and displayed on the Tera Term software.

As a result, we have successfully transmitted the PPG signals via Bluetooth from a reflectance organic pulse meter and measured the heart rate from the signals. Device-C successfully showed a very clear PPG signal on the receiving PC host. Figure 5.6A shows the wireless PPG waveform on our C# program where the data were obtained from the USB dongle that supported BLE. The role of the USB dongle is to convert the Bluetooth signal to a COM port serial signal. Therefore, the dongle was needed in the case that the PC did not have a built-in Bluetooth or did not support the BLE. PPG waveform was recorded from the program as a comma-separated values (CSV) file and is presented in Figure 5.6B. It is noteworthy to mention that the PPG signals encounter several factors that can influence the signal's quality, such as the amount of pressure from the human body against OLED/OPD device substrate. The device substrate should be coupled with the skin in order to receive the reflected light on the OPD. However, more pressure on the skin results in more pressure on the blood vessels, and that causes weakness of the PPG signal's amplitude. Therefore, moderate pressure from the human body should be applied to the pulse meter's substrate.

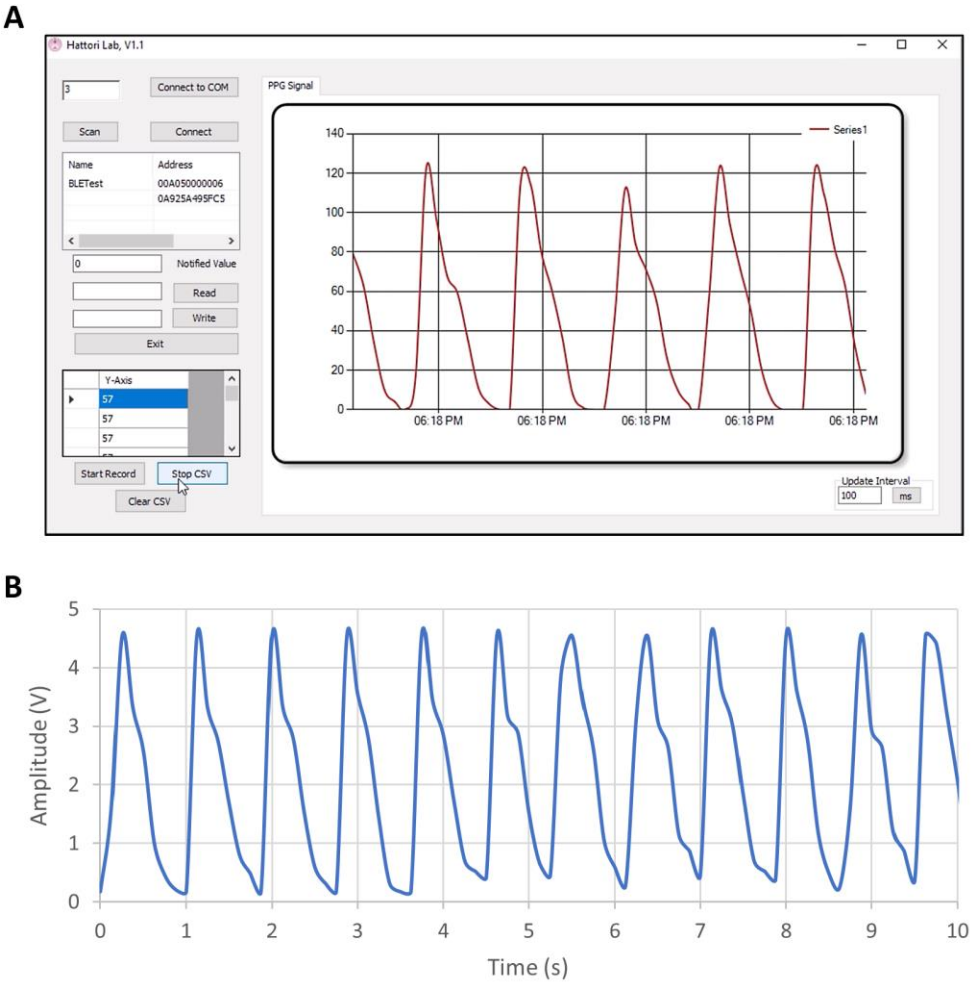

Figure 5.6: (**A**) The C# program shows PPG signal obtained from a universal serial bus (USB) dongle that was connected to the portable pulse meter via BLE; (**B**) PPG waveform after being recorded from the program as a comma-separated values (CSV) file.

5.5 SUMMARY

This chapter has shown the performance and accuracy results of the proposed system. Results from three different design structures of the three devices were compared and discussed. Furthermore, the chapter discussed the results of the obtained PPG signal from several parts of the body along with comparing the PPG signal that has been acquired wirelessly from the BLE.

CHAPTER SIX:

CONCLUSIONS AND FUTURE WORK

6.1 CONCLUSIONS

A pulse oximetry sensor has become essential to medical electronics and wearable health monitoring devices. It is a noninvasive, inexpensive, convenient, and safe device for monitoring a person's health and avoiding any potential illness. The pulse oximeter is used to determine physiological parameters such as heart rate (bpm) and peripheral oxygen saturation (SpO_2) of patients at all times based on the photoplethysmogram (PPG) method. PPG signal is an essential bio-signal that can be used for detecting several heart diseases. It has become fundamental to wearable health monitoring devices. There are various kinds of commercial pulse meter and pulse oximeter devices available on the market. However, there are still some issues in these kinds of pulse meters which need to be improved in some performances such as the power consumption and the flexibility of the device.

This research project aims to fabricate organic light-emitting diode (OLED) and organic photodiode (OPD) biosensors, minimize the power consumption of the organic optoelectronic pulse meter sensor, develop the driver circuit of the pulse meter, improves the PPG bio-signal quality and proposes a reliable pulse meter instrument that can be used in Vivo physiological monitoring. It also implements Bluetooth low energy (BLE) for sending the PPG waveform wirelessly to a mobile phone or a PC host. The thesis consists of six chapters organized as follows:

Chapter 1 begins by giving a brief overview of the study, motivation and problem statement, objectives of the research and followed by the research methodology.

Chapter 2 comprises literature review and related works, where the previous works on pulse oximeter systems, PPG principle, reflective type, transmissive type, organic optoelectronic, driving circuits, and digital filters are discussed in detail.

Chapter 3 discusses the results of the optical simulation that leads to the best design structure in terms of power consumption and signal quality. Following that, the proposed design structure of the organic optoelectronic pulse meter and the characteristics of the device performance are presented.

Chapter 4 discusses the system design developed for the proposed organic pulse meter. The driver circuit and its stages were explained thoroughly. It also illustrates the approach of measuring the SNR, the algorithm for measuring the heart rates, the data traffic of the BLE, and designing the digital filter that applied to the system.

Chapter 5 contains the results of the proposed system's performance and accuracy. It compares the proposed design structures and discusses the results of the obtained PPG signal from several parts of the body along with comparing the PPG signal that acquired wirelessly via BLE.

Chapter 6 presents the outcomes of the work presented in this dissertation. Thesis contribution to the current state of knowledge, recommendations, and future work are also presented.

Two approaches can be used to obtain a PPG signal from a biosensor pulse meter: reflection and transmission. The reflection method was adopted in this research because of the freedom of use. The device could be easily worn or attached to different parts of the human body. The transmission method involved tissue transillumination and required that a light source and a detector be placed opposite each other. Consequently, the transmission method could only be used on external body parts such as fingertips, toes, and ear lobes.

The thesis addressed the significance of designing an effective OLED and OPD structure to improve pulse meter sensors in terms of power consumption and signal quality. Designing an OLED that emits a high amount of light is not necessary to produce a high-quality PPG signal; instead, it will consume more power. On the other hand, designing an effective OLED and OPD structure guided by optical simulation led to the best result in terms of power consumption and signal quality. That assumption was verified by comparing three different pulse meter design structures. One device had a circle-shaped OLED in the center of the device and was surrounded by a ring-shaped OPD, while the second device had the opposite structure. The third device had a bigger OLED area and a shorter distance gap between the OLED and the OPD. The devices were simulated optically where the simulator traced one million rays in each device. The simulation results showed the irradiance on the OPD area, where the maximum estimated irradiances were 3.7×10^{-10} W/mm^2, 2 x10^{-9} W/mm^2 and 9.8×10^{-10} W/mm^2 as a total received power of 0.42%, 0.1%, and 0.55% for Device-A, Device-B and Device-C, respectively.

The gap distance between the OLED and the OPD showed a top priority while designing an organic pulse meter along with the OLED's area and OPD's area. At low current source for OLED, the larger gap will result in reducing the SNR, while the shorter gap between the OLED and the OPD devices will result in improving the SNR where the chance of obtaining more reflected light is increased. Whereas in the high current source for OLED, decreasing the distance of the gap between the OLED and the OPD leads to an increase in the DC noise on the OPD.

The OLED's area and OPD's area should also be taken into consideration while designing an organic pulse meter. For the OLED's area, if we reduced the OLED's area in order to reduce the power consumption, the OLED's lifetime will also be reduced

because the current density will be increased in a small area. On the other hand, if the OLED's area increased, then the area in the center of the OLED will be impractical and will not contribute to increasing the reflected light from the human body. For designing the OPD's area, it should be designed in a way to surround the OLED sufficiently in order to collect more reflected light. However, increasing the OPD's area too much will result in increasing the DC noise. Therefore, the area of the OPD should be consistent with OLED design, which can be achieved by optical simulation.

Red OLEDs, 625 nm, and OPDs sensitive at the aforementioned wavelength were fabricated monolithically on glass substrates. The external quantum efficiency (EQE) of the OLED and the OPD were 7% and 37%, respectively. The power consumption and the signal-to-noise ratio (SNR) were evaluated for all devices' PPG signals, which were successfully acquired from fingertips and other body parts. Accordingly, the proposed reflectance-based organic pulse meter operated successfully at an ultra-low power consumption of 8 μW at 18 dB SNR and low power consumption of 0.1 mW at 62 dB.

The proposed organic pulse meter was implemented for wireless monitoring of the PPG signal and successfully presented compatible characteristics. Clear PPG waveforms were obtained from the portable pulse meter via Bluetooth low energy (BLE) at 500 SPS and 8-bit resolution on the receiver PC host. The maximum throughput data rate between the chip and the PC host was 256 kbps at the minimum connection interval of 7.5 ms. The proposed pulse meter showed accurate results of about 1.5% error of the pulse rate (PR) compared to the commercially reference we obtained. Eventually, the proposed organic biosensor reduced the power consumption and improved the capability of the pulse meter for long-term use.

6.2 CONTRIBUTION OF THE THESIS

This research project aimed to fabricate OLED/OPD biosensors, improve the PPG bio-signal quality, and propose a reliable pulse-meter instrument that can be used in Vivo physiological monitoring. It also implemented BLE for sending the PPG waveform wirelessly to a mobile phone or a PC host.

Secondly, the thesis presented the significance of designing an effective OLED and OPD structure that was guided by optical simulation for improving pulse meter sensors in terms of power consumption and signal quality.

Thirdly, reducing the power consumption and improving the noise level of the biosensors were significant factors for improving the reliability of the pulse-meters to be used as a wearable medical device. This work improved the PPG signal quality to about 45 dB without digital filter and more than 62 dB after applying FIR digital filter. It also minimized the power consumption of the OLED to ultra-low power consumption of 8 µW at 18 dB SNR and low power consumption of 0.1 mW at 62 dB.

6.3 FUTURE WORK

Despite the successful results of the proposed organic optoelectronic pulse meter, more aspects of the pulse meter need to be considered in order to enhance the pulse meter system, which are suggested as follows:

- A green OLED to be fabricated along with red OLED in order to make a pulse oximeter device.
- OLED and OPD to be fabricated on a flexible substrate to increase the pulse meter's reliability and flexibility of use as a comfortable wearable device for medical applications.

- In order to get a high PPG signal quality, it is recommended to use the reflective pulse meter on body parts that have less density of fat such as the fingertips, wrist, arms, neck, and forehead.
- The NIR OLED can be used instead of the green OLED to estimate the SpO_2 where the NIR OLED has a longer wavelength which leads to increasing the penetration depth of the light in the human body and produce higher quality PPG signal, but the materials of the NIR OLED/OPD device are still under research and development due to instability issues.
- When using the pulse meter with more pressure on the skin, it will result in more pressure on the blood vessels, and that causes weakness of the PPG signal's amplitude. Therefore, moderate pressure on the human body should be applied from the pulse meter.

REFERENCES

1. Yoon, S.; Cho, Y.H. A skin-attachable flexible piezoelectric pulse wave energy harvester. *J. Phys. Conf. Ser.* **2014**, *557*.

2. Buxi, D.; Penders, J.; Van Hoof, C. Early results on wrist based heart rate monitoring using mechanical transducers. *2010 Annu. Int. Conf. IEEE Eng. Med. Biol. Soc. EMBC'10* **2010**, 4407–4410.

3. Webster, J.G. *Design of Pulse Oximeters*; CRC Press, 1997;

4. Jubran, A. Pulse oximetry. *Appl. Physiol. Intensive Care Med. 1 Physiol. Notes - Tech. Notes - Semin. Stud. Intensive Care, Third Ed.* **2012**, 51–54.

5. Guk, K.; Han, G.; Lim, J.; Jeong, K.; Kang, T. Evolution of Wearable Devices with Real-Time Disease Monitoring for Personalized Healthcare. **2019**, 1–23.

6. Khan, Y.; Ostfeld, A.E.; Lochner, C.M.; Pierre, A.; Arias, A.C. Monitoring of Vital Signs with Flexible and Wearable Medical Devices. *Adv. Mater.* **2016**, *28*, 4373–4395.

7. Chen, C.T. Evolution of red organic light-emitting diodes: Materials and devices. *Chem. Mater.* **2004**, *16*, 4389–4400.

8. Thejo Kalyani, N.; Dhoble, S.J. Organic light emitting diodes: Energy saving lighting technology - A review. *Renew. Sustain. Energy Rev.* **2012**, *16*, 2696–2723.

9. Geffroy, B.; le Roy, P.; Prat, C. Organic light-emitting diode (OLED) technology: Materials, devices and display technologies. *Polym. Int.* **2006**, *55*, 572–582.

10. Evans, D.; Hodgkinson, B.; Berry, J. Vital signs in hospital patients: A systematic review. *Ijns* **2001**, *38*, 643–650.

11. LoCicero, R. Anemia: MedlinePlus Medical Encyclopedia. *A.D.A.M., Inc.* 2017.

12. Fox, S.I. *Human Physiology, FOURTEENTH EDITION*; McGrawHill: New York, 2016;

13. Prahl, S. Optical Absorption of Hemoglobin. *https://omlc.org/spectra/hemoglobin/* **1999**.

14. de Kock, J.P.; Tarassenko, L. Pulse oximetry: theoretical and experimental models. *Med. Biol. Eng. Comput.* **1993**, *31*, 291–300.

15. Wukitsch, M.W.; Petterson, M.T.; Tobler, D.R.; Pologe, J.A. Pulse oximetry, analysis of theory, technology, and practice. **1988**, *4*, 290–301.

16. Kamat, V. Pulse Oximetry. *Indian J. Anaesth.* **2002**, *46*, 261–268.

17. Jorgensen, J.S.; Schmid, E.R.; Knig, V.; Faisst, K.; Huch, A.; Huch, R. *Limitations of forehead pulse oximetry*; 1995; Vol. 11, pp. 253–256;.

18. Shelley, K.; Shelley, S. Pulse oximeter waveform: photoelectric plethysmography. *Clin. Monit. Pract. Appl. Anesth. Crit. care* **2001**, 420–8.

19. Reisner, A.; Shaltis, P.A.; McCombie, D.; Asada, H.H. Utility of the photoplethysmogram in circulatory monitoring. *Anesthesiology* **2008**, *108*, 950–958.

20. Allen, J. Photoplethysmography and its application in clinical physiological measurement. *Physiol. Meas.* **2007**, *28*, 1–39.

21. Lee, H.; Ko, H.; Lee, J. Reflectance pulse oximetry: Practical issues and limitations. *ICT Express* **2016**, *2*, 195–198.

22. Chung, S.C.; Sun, C.C. Signal-enhancement reflective pulse oximeter with Fresnel lens. *Opt. Commun.* **2016**, *375*, 9–14.

23. Mendelson, Y.; Pujary, C. Measurement site and photodetector size considerations in optimizing power consumption of a wearable reflectance pulse oximeter. *Annu. Int. Conf. IEEE EMBS* **2004**, 3016–3019.

24. Ha, M.; Lim, S.; Ko, H. Flexible Health-Monitoring Devices/Sensors. In *Flexible and Stretchable Medical Devices*; 2018; pp. 287–289.

25. Lochner, C.M.; Khan, Y.; Pierre, A.; Arias, A.C. All-organic optoelectronic sensor for pulse oximetry. *Nat. Commun.* **2014**, *5*, 1–7.

26. Khan, Y.; Han, D.; Pierre, A.; Ting, J.; Wang, X.; Lochner, C.M.; Bovo, G.; Yaacobi-Gross, N.; Newsome, C.; Wilson, R.; et al. A flexible organic reflectance oximeter array. *Proc. Natl. Acad. Sci.* **2018**, *115*, E11015–E11024.

27. Tachibana, Y.; Kaltenbrunner, M.; Koizumi, M.; Matsuhisa, N.; Yukita, W.; Zalar, P.; Jinno, H.; Someya, T.; Kitanosako, H.; Yokota, T. Ultraflexible organic photonic skin. *Sci. Adv.* **2016**, *2*, e1501856.

28. Kim, H.; Lee, H.; Yoo, S.; Kim, M.; Kim, E.; Lee, J.; Yoo, H.-J.; Lee, Y. Toward all-day wearable health monitoring: An ultralow-power, reflective organic pulse oximetry sensing patch. *Sci. Adv.* **2018**, *4*, eaas9530.

29. Elsamnah, F.; Bilgaiyan, A.; Muhamad, A.; Shim, C. Reflectance-Based Organic Pulse Meter Sensor for Wireless Monitoring of Photoplethysmogram Signal. *Biosensors* **2019**, *9*, 87.

30. Elsamnah, F.; Bilgaiyan, A.; Affiq, M.; Shim, C.-H.; Ishidai, H.; Hattori, R. Comparative Design Study for Power Reduction in Organic Optoelectronic Pulse Meter Sensor. *Biosensors* **2019**, *9*, 48.

31. Bilgaiyan, A.; Sugawara, R.; Elsamnah, F.; Shim, C.; Affiq, M.; Hattori, R. Optimizing performance of reflectance-based organic Photoplethysmogram (PPG) sensor. In Proceedings of the Organic and Hybrid Sensors and Bioelectronics XI; 2018; Vol. 10738, p. 1073808.

32. Elsamnah, F.; Hattori, R.; Shim, C.-H.; Bilgaiyan, A.; Sugawara, R.; Affiq, M. Reflectance-based Monolithic Organic Pulsemeter Device for Measuring Photoplethysmogram Signal. *2018 IEEE Int. Instrum. Meas. Technol. Conf.* **2018**, 1–5.

33. Rodrigues, E.M.G.; Godina, R.; Cabrita, C.M.P.; Catalão, J.P.S. Experimental low cost reflective type oximeter for wearable health systems. *Biomed. Signal Process. Control* **2017**, *31*, 419–433.

34. Amplifier, E.T.; Tavakoli, M.; Member, S.; Turicchia, L.; Sarpeshkar, R.; Member, S. An Ultra-Low-Power Pulse Oximeter Implemented. *IEEE Trans. Biomed. Circuits Syst.* **2010**, *4*, 27–38.

35. Glaros, K.N.; Drakakis, E.M. A Sub-mW fully-integrated pulse oximeter front-

end. *IEEE Trans. Biomed. Circuits Syst.* **2013**, *7*, 363–375.

36. Li, K.; Warren, S. A wireless reflectance pulse oximeter with digital baseline control for unfiltered photoplethysmograms. *IEEE Trans. Biomed. Circuits Syst.* **2012**, *6*, 269–278.

37. Ayance, T.; Trevi, C.G. Wireless heart rate and oxygen saturation monitor Wireless Heart Rate and Oxygen Saturation Monitor. **2019**, *040010*, 1–5.

38. Huang, C.; Chan, M.; Chen, C.; Lin, B. Novel Wearable and Wireless Ring-Type Pulse Oximeter with Multi-Detectors. **2014**, 17586–17599.

39. Spigulis, J.; Erts, R.; Nikiforovs, V.; Kviesis-kipge, E. Wearable wireless photoplethysmography sensors. **2008**, *6991*, 1–7.

40. Kabir, M.A.; Shahnaz, C. Denoising of ECG signals based on noise reduction algorithms in EMD and wavelet domains. *Biomed. Signal Process. Control* **2012**, *7*, 481–489.

41. Kim, B.S.; Yoo, S.K. Motion Artifact Reduction in Photoplethysmography Using Independent Component Analysis. *IEEE Trans. Biomed. Eng.* **2006**, *53*, 566–568.

42. Sun, X.; Yang, P.; Zhang, Y.-T. Assessment of photoplethysmogram signal quality using morphology integrated with temporal information approach. In Proceedings of the Engineering in Medicine and Biology Society (EMBC), 2012 Annual International Conference of the IEEE; 2012; pp. 3456–3459.

43. Waugh, W.; Allen, J.; Wightman, J.; Sims, A.J.; Beale, T.A.W.W. Novel signal noise reduction method through cluster analysis , applied to photoplethysmography. *Comput. Math. Methods Med.* **2017**, *2018*, 1–17.

44. Rundo, F.; Conoci, S.; Ortis, A.; Battiato, S. An advanced bio-inspired photoplethysmography (PPG) and ECG pattern recognition system for medical assessment. *Sensors (Switzerland)* **2018**, *18*.

45. Jacques, S.L. Optical properties of biological tissues: a review. *Phys. Med. Biol.* **2013**, *58*, R37.

46. Zamburlini, M.; Pejović-Milić, A.; Chettle, D.R.; Webber, C.E.; Gyorffy, J. In vivo study of an x-ray fluorescence system to detect bone strontium non-

invasively. *Phys. Med. Biol.* **2007**, *52*, 2107–2122.

47. Akkus, O.; Uzunlulu, M.; Kizilgul, M. Evaluation of Skin and Subcutaneous Adipose Tissue Thickness for Optimal Insulin Injection. *J. Diabetes Metab.* **2012**, *03*.

48. Drahansky, M.; Kanich, O.; Brezinová, E.; Shinoda, K. Experiments with Optical Properties of Skin on Fingers. *Int. J. Opt. Appl.* **2016**, *6*, 37–46.

49. Anderson, R.R.; Parrish, J.A. The optics of human skin. *J. Invest. Dermatol.* **1981**, *77*, 13–19.

50. Tamura, T.; Maeda, Y.; Sekine, M.; Yoshida, M. Wearable Photoplethysmographic Sensors—Past and Present. *Electronics* **2014**, *3*, 282–302.

51. Sommer, J.R.; Farley, R.T.; Graham, K.R.; Yang, Y.; Reynolds, J.R.; Xue, J.; Schanze, K.S. Efficient Near-Infrared Polymer and Organic Light-Emitting Diodes Based on Electrophosphorescence from. **2009**, *1*.

52. Xue, J.; Li, C.; Xin, L.; Duan, L.; Qiao, J. High-efficiency and low efficiency roll-off near-infrared fluorescent OLEDs through triplet fusion. **2016**, 2888–2895.

53. World Famous Electronics llc Heartbeats in Your Project Available online: https://pulsesensor.com/ (accessed on Jan 9, 2018).

54. Broadcom Inc. Miniature Surface-Mount Ambient Light Photo Sensor Available online: https://www.broadcom.com/docs/AV02-1169EN (accessed on Jul 1, 2019).

55. Jung, S.; Cressler, J.D.; Babcock, J.A.; Cestra, G.; Buchholz, A. A design methodology to achieve low input impedance and non-constant gain-bandwidth product in TIAs for optical communication. *Proc. - IEEE Int. Symp. Circuits Syst.* **2013**, *3*, 598–601.

56. Park, S.M.; Toumazou, C. Low Noise Current-Mode CMOS Transimpedance Amplifier for Giga-bit Optical Communication. *ISCAS '98. Proc. 1998 IEEE Int. Symp. Circuits Syst. (Cat. No.98CH36187)* **1998**, *1*, 293–296.

57. Bluetooth SIG Bluetooth Technology Website Available online: http://www.bluetooth.com.

58. Texas Instruments Bluetooth® low energy Beacons Available online: http://www.ti.com/lit/an/swra475a/swra475a.pdf.

59. Luthra, G. PROJECT #024: BLE Throughput - Pushing the Limits Available online: http://www.cypress.com/blog/100-projects-100-days/project-024-ble-throughput-pushing-limits (accessed on Jun 10, 2019).

60. Gautam, G.; Shrestha, S.; Cho, S. Spectral Analysis of Rectangular , Hanning , Hamming and Kaiser Window for Digital Fir Filter. **2015**, *4*, 138–144.

61. Raz Ghulam Ahmad, A.M.J. Design and Performance Analysis of Low Pass Fir Filter Using Hamming and Kaiser Windows. **2014**, 8676–8683.

62. Sun, X.; Yang, P.; Li, Y.; Gao, Z.; Zhang, Y.-T. Robust heart beat detection from photoplethysmography interlaced with motion artifacts based on empirical mode decomposition. In Proceedings of the Proceedings of 2012 IEEE-EMBS International Conference on Biomedical and Health Informatics; 2012; pp. 775–778.

63. Xu, L.; Zhang, D.; Wang, K.; Li, N.; Wang, X. Baseline wander correction in pulse waveforms using wavelet-based cascaded adaptive filter. *Comput. Biol. Med.* **2007**, *37*, 716–731.

64. Vadrevu, S.; Manikandan, M.S. A Robust Pulse Onset and Peak Detection Method for Automated PPG Signal Analysis System. *IEEE Trans. Instrum. Meas.* **2018**, *PP*, 1–11.

65. Shin, H.S.; Lee, C.; Lee, M. Adaptive threshold method for the peak detection of photoplethysmographic waveform. *Comput. Biol. Med.* **2009**, *39*, 1145–1152.

66. Kavsaoğlu, A.R.; Polat, K.; Bozkurt, M.R. An innovative peak detection algorithm for photoplethysmography signals: An adaptive segmentation method. *Turkish J. Electr. Eng. Comput. Sci.* **2016**, *24*, 1792–1796.

PUBLICATIONS

1) **F. Elsamnah**, A. Bilgaiyan, M. Affiq, C.-H. Shim, H. Ishidai, and R. Hattori, "Reflectance-based Organic Pulse Meter Sensor for Wireless Monitoring the Photoplethysmogram Signal," *Biosensors*, vol. 9, no. 3, p. 87, 2019.

2) **F. Elsamnah**, A. Bilgaiyan, M. Affiq, C.-H. Shim, H. Ishidai, and R. Hattori, "Comparative Design Study for Power Reduction in Organic Optoelectronic Pulse Meter Sensor," *Biosensors*, vol. 9, no. 2, p. 48, 2019.

3) A. Bilgaiyan, R. Sugawara, **F. Elsamnah**, C. Shim, M. Affiq, and R. Hattori, "Optimizing performance of reflectance-based organic Photoplethysmogram (PPG) sensor," in *Organic and Hybrid Sensors and Bioelectronics XI*, 2018, vol. 10738, p. 1073808.

4) **F. Elsamnah**, R. Hattori, C.-H. Shim, A. Bilgaiyan, R. Sugawara, and M. Affiq, "Reflectance-based Monolithic Organic Pulsemeter Device for Measuring Photoplethysmogram Signal," *2018 IEEE Int. Instrum. Meas. Technol. Conf.*, pp. 1–5, 2018.

5) **F. Elsamnah**, R. Hattori, C.-H. Shim, A. Bilgaiyan, R. Sugawara, and M. Affiq, "Detecting Circuit for Organic Pulse Oximetry," in International Exchange and Innovation Conference on Engineering & Sciences (IEICES), 2017, pp. 53–56.